JOURNAL OF GEOPHYSICAL RESEARCH, VOL. 100, NO. B11, PAGES 22,133–22,154, NOVEMBER 10, 1995

The rupture zone of Cascadia great earthquakes from current deformation and the thermal regime

R.D. Hyndman and K. Wang

Pacific Geoscience Centre, Geological Survey of Canada, Sidney, British Columbia

Abstract. An important but poorly known part of the earthquake hazard at near-coastal cities of western North America from southern British Columbia to northern California is from great thrust earthquakes on the Cascadia subduction zone. Although there have been no such events in the historical record, there is good geological evidence that they have occurred in the past. The downdip landward limit of the seismogenic or seismic rupture zone on the subduction thrust fault has been estimated for the whole Cascadia margin from (1) the locked zone from dislocation modeling of current deformation data, and (2) the thermal regime, taking the downdip limit of seismic behavior on the fault to be controlled by temperature. The geodetic data include ten leveling lines, tide gauges at six locations along the coast, one high precision gravity line, seven horizontal strain arrays, and a continuously recording Global Positioning System (GPS) network. There is present uplift for most of the coast at a rate of a few millimeters per year, decreasing inland, and shortening across the coastal region at about 0.1 μstrain/yr (i.e., 10 mm/yr over a distance of 100 km). The present interseismic uplift is consistent with the great earthquake coseismic subsidence inferred from buried coastal salt marshes and other paleoseismicity data. The modeled width of the locked zone that is taken to be accumulating elastic strain averages 60 km fully locked, plus 60 km transition (90 km fully locked with no transition gives similar interseismic deformation). It is wider off the Olympic Peninsula of northern Washington and narrower off central Oregon to northern California. This unusually narrow downdip extent compared to many other subduction zones is a consequence of high temperatures associated with the young oceanic plate and the thick blanket of insulating sediments on the incoming crust. The variations in the modeled locked zone from geodetic data correspond well to variations along the margin of downdip temperatures on the fault as estimated from numerical thermal models, taking the maximum temperature for the fully locked seismogenic zone to be 350°C with a transition zone to 450°C. The temperatures on the subduction thrust fault and thus the downdip extent of the seismogenic zone depend on five local subduction parameters: (1) the age of the subducting plate, (2) the plate convergence rate, (3) the thickness of insulating sediments on the incoming crust, (4) the dip angle profile of the fault, and (5) the thermal properties of the overlying material. The landward limit to the seismogenic zone, extending little if at all beneath the coast, limits the ground motion from great subduction earthquakes at the larger Cascadia cities that lie 100-200 km inland. The narrow width also limits the earthquake size but events of magnitude well over 8 are still possible; the maximum depends on the along-margin length. If the whole Cascadia margin seismogenic zone fails in a single event, empirical fault area versus magnitude relations give earthquakes as large as M_w=9.

Introduction

The Cascadia subduction zone margin of western North America (Figure 1) is unusual in having experienced no historical great thrust earthquakes. However, most comparable margins globally have had such very damaging events and extensive paleoseismicity data from sites along the coast from southern Vancouver Island to northern California indicate that they have occurred at irregular intervals averaging about 600 years. The last event was 300 years ago [e.g., *Atwater et al.*, 1995; *Clague and Bobrowsky*, 1994a, b; *Atwater*, 1990; *Adams*, 1990]. Current uplift of the coastal areas at rates of a few millimeters per year has been defined from a variety of data. This contrasts with the interseismic coastal subsidence and coseismic uplift observed for most subduction zones elsewhere that have experienced great earthquakes. Consequently, it was earlier concluded that Cascadia subduction is aseismic [e.g., *Ando and Balazs*, 1979]. *Savage et al.* [1981], however, first showed from repeated trilateration surveys that there was shortening across the margin of the Olympic Peninsula that could not easily be explained by aseismic subduction and that a narrow locked zone could result in the observed interseismic coastal uplift. Subsequent positional and vertical surveys have substantiated the conclusion of a locked thrust and this

Published in 1995 by the American Geophysical Union.

Paper number 95JB01970.

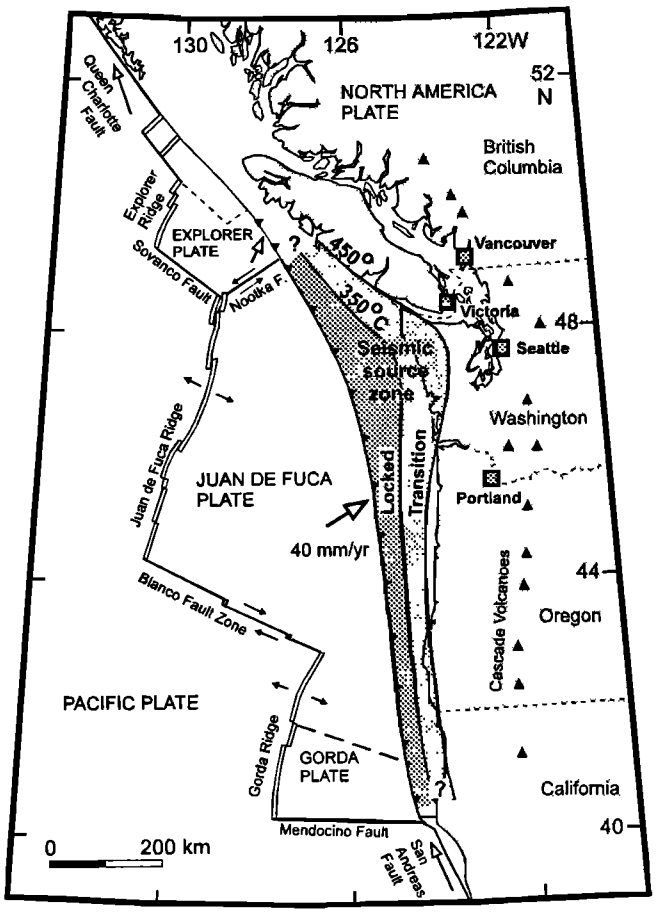

Figure 1. The Cascadia margin of western North America. The plan view of the locked and transition zones on the subduction thrust fault estimated from dislocation modeling of the current deformation are dark and light stippled respectively. The model great earthquake rupture extends with decreasing displacement to the landward limit of the transition zone. The downdip limits correspond approximately to the 350°C and 450 °C isotherms respectively. Plate motions are with respect to the North American plate.

conclusion is now generally accepted [e.g., *Dragert et al.*, 1994]. In this article we review and model a variety of geodetic data to estimate the downdip extent of the locked subduction thrust fault that is accumulating elastic strain. We also report on the results of a series of thermal sections across the margin generated using numerical models, motivated by the inference that the downdip extent is thermally limited. At greater than a critical temperature, stable sliding or plastic deformation must occur. Agreement between the deformational and thermal constraints gives confidence that the seismogenic zone has been accurately defined. The downdip limit of the locked fault corresponds to the landward extent of the seismic source zone and thus is an important factor in the seismic hazard inland. The width of the source zone also provides a general constraint to the maximum earthquake magnitude. There is now evidence that (1) the width of the interseismic locked zone obtained from elastic dislocation modeling of vertical and horizontal geodetic data and (2) the seismogenic width from thermal constraints, both correspond well to the maximum downdip limit of coseismic rupture in great subduction zone earthquakes. This agreement was shown in a detailed comparison for southwest Japan where there is considerable seismic and tsunami data for historical great earthquakes [*Hyndman et al.*, 1995].

For the northern portion of the Cascadia margin at Vancouver Island, previous comparisons of geodetic data with elastic and viscoelastic dislocation models indicated that the locked seismogenic zone is only about 60 km wide fully locked, plus a 60 km transition zone [*Dragert et al.*, 1994; *Wang et al.*, 1994]. We have concluded that the unusually narrow width is a consequence of high temperatures resulting from the young age of the subducting lithosphere and the thick blanket of insulating sediments on the incoming oceanic crust [*Hyndman and Wang*, 1993]. Previous modeling of current deformation data and thermal modeling have indicated that the locked zone is wider across the Olympic Peninsula of northern Washington, but otherwise farther to the south it is roughly similar to that off Vancouver Island [e.g., *Hyndman and Wang*, 1993; *Savage et al.*, 1991; *Dragert and Hyndman*, 1995].

Important new data are now available for dislocation modeling; *Mitchell et al.* [1994] have presented recently repeated leveling data and long term tide gauge trends for the Washington and Oregon margins (also *Mitchell* [1992] and *Vincent* [1989]). This addition to extensive older data allows the width of the locked zone for the whole Cascadia margin to be estimated. A variety of new structural and thermal data also allow comparison of the geodetically estimated locked zone with that from thermal constraints.

Current Deformation Constraints of the Locked Zone

If a portion of the subduction thrust fault is locked, ongoing convergence results in the toe of the continent being dragged down and the formation of a flexural uplift bulge farther inland

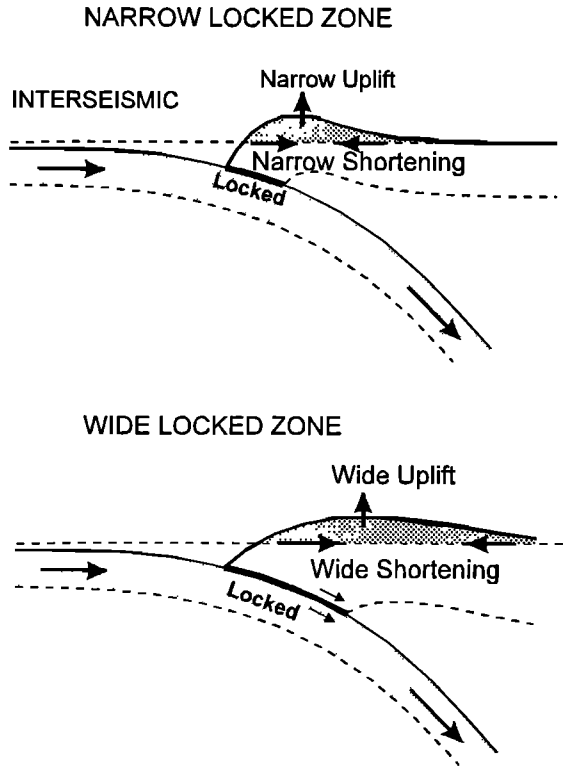

Figure 2. A schematic diagram illustrating the pattern of interseismic vertical and horizontal deformation for a locked subduction thrust fault. The wider the locked zone the farther the region of uplift extends landward. The coseismic deformation is approximately the inverse.

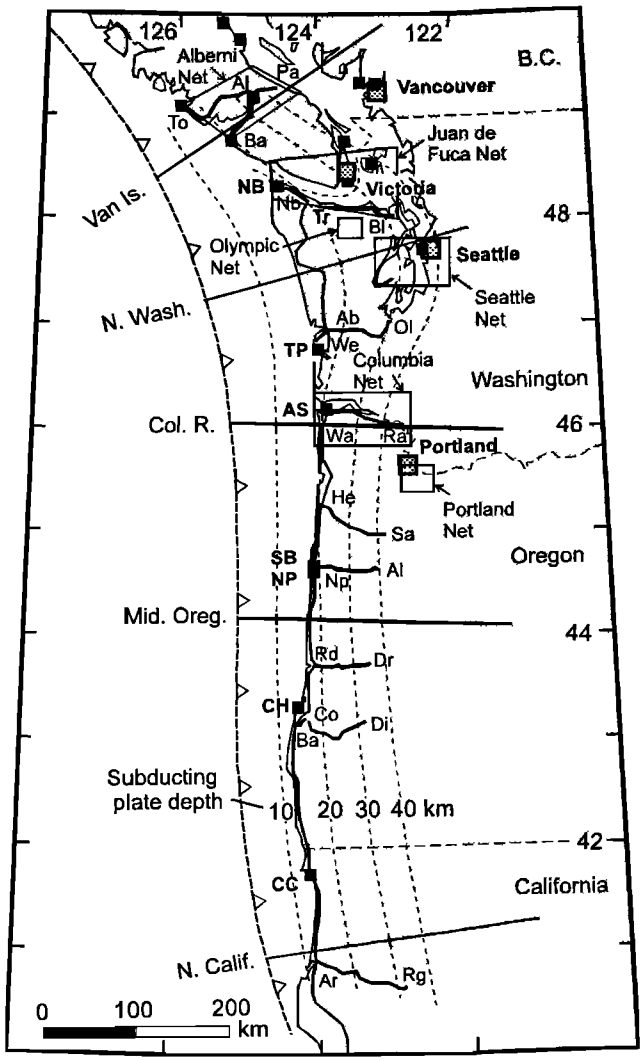

Figure 3. The Cascadia margin study area. The dashed lines are the contours of subducting plate depth; they are poorly constrained for Oregon. The thick solid lines are the leveling lines studied and the small solid squares are the tide gauge sites modeled in this article. The location abbreviations are identified in the tables and text. The thin line boxes enclose the areas of the positional surveys. The thick straight lines perpendicular to the deformation front are the five deformation model profiles.

along with elastic crustal shortening (Figure 2). The wider the locked zone, the farther landward are the flexural uplift and the transition between interseismic subsidence and uplift. Thus matching the spatial pattern of vertical motion and horizontal shortening across the margin from geodetic data with that from deformation models allows the width of the locked and thus seismogenic zone to be estimated. Great earthquakes may rupture all or some portion of this seismogenic zone.

Five types of geodetic data are available to define the pattern of current deformation across the Cascadia margin: (1) repeated survey leveling lines, (2) long-term trends in tide gauge data, (3) a repeated precision gravity survey, (4) repeated positional survey networks, and (5) a continuously recording Global Positioning (GPS) network (Figure 3). The most comprehensive surveys that constrain the width of the locked zone are across the northern Cascadia margin at southern Vancouver Island where all five types of current deformation data are available [*Dragert et al.*, 1994; *Dragert and Hyndman*, 1995]. The model that best fits the data has a 60-km-wide locked zone plus a 60-km-wide transition zone. This result is in good agreement with the width of the seismogenic zone from detailed thermal modeling at this location [*Hyndman and Wang*, 1993]. We continue a similar analysis of geodetic and thermal data for the remainder of the Cascadia margin in this article.

Analyses of uplifted shore platforms formed 80-120 kyr ago indicate long-term uplift rates of less than 0.2 mm/yr except in a few local areas of folding and faulting [*Kelsey et al.*, 1994, and references therein]. This is more than a factor of 10 smaller than most of the geodetically measured rates. Thus the net motion over many earthquake cycles is negligible compared to the interseismic rates. We assume that there is also approximately zero net displacement for individual earthquake cycles based on data for some other areas [e.g., *Hyndman et al.*, 1995], although this has yet to be established for Cascadia.

Repeated leveling by the U.S. National Geodetic Survey and the Geodetic Survey of Canada on a number of profiles across the margins of British Columbia, Washington, Oregon, and northern California have been presented by *Ando and Balazs* [1979], *Reilinger and Adams* [1982], *Dragert and Lisowski* [1990], *Holdahl et al.* [1989], *Dragert et al.* [1994], and *Mitchell et al.* [1994]. J. Adams (personal communication, 1994) has provided us with additional older data. General uplift of the coastal areas at rates of a few millimeters per year has been defined. A summary of the available lines is given in Table 1; the data are presented in comparison with models in the next section. The repeated leveling and gravity data provide only relative levels, and they have been referenced to the tide gauge data and to margin-parallel leveling lines [*Dragert et al.*, 1994; *Mitchell et al.*, 1994]. The vertical data have also been corrected for postglacial rebound. A correction of 1 mm/yr has been applied to the tide gauge data, and thus indirectly to the leveling data, for the central and southern parts of the study area where there are small spatial gradients in estimated rebound [*Peltier*, 1986; T. James, personal communication, 1995]. For the northern area where there are horizontal gradients in postglacial rebound of up to 2 mm/yr along the ~100 km lengths of the leveling lines, the corrections are as given by *Dragert et al.* [1994]. The corrected vertical reference levels have uncertainties of about 1.0 mm/yr. For the northern lines where there is a significant gradient in postglacial rebound, there is also a tilt uncertainty of about 1 mm/yr between the ends of the leveling lines. The corrected repeated leveling and gravity profiles exhibit approximately zero vertical motion at their landward ends as predicted by our simple elastic dislocation models.

The propagation of errors along the leveling lines (the landwardmost points are taken as fixed) has been estimated from the survey specifications. Most of the surveys are to first order requirements, for which the error estimate is 4 mm·$K^{1/2}$, where K is the survey line distance [*Brown and Oliver*, 1976; *Vanicek et al.*, 1980]. As pointed out by *Vanicek et al.* [1980], there are probably error correlations between two levelings of the same route, so the difference error may be less. However, for the longer time intervals, larger errors are expected because of different survey specifications for successive surveys. Most of the rate variations over short distances (<20 km) along the leveling lines are within the error estimates and thus are not significant. The few points that are substantially off the general trends of the profiles are assumed to represent unstable bench marks. They have been ignored in determining the best fitting models. The first-order error estimate gives relative errors between the ends of 100-km lines ranging from ±0.7 mm/yr for

Table 1a. Tide Gauge Data for the Cascadia margin

Gauge	Distance from Base of Slope, km	Land Uplift mm/yr±1 s.e.	Corrected for Sealevel Rise	Corrected for Postglacial Rebound	References [a]
Neah Bay (NB)	140 (165) [b]	1.6±0.2	3.4	3.4	1,2,(3),4
Toke Point (TP)	133	0.2 (-2.1) [c]	2.0	3.0 (-0.3) [c]	4
Astoria (AS)	131	0.0±0.2	1.8	2.8	2,(4)
Newport/ South Beach (NP/SB)	99	-2.2±0.4	-0.4	0.6	4
Charleston (CH)	74	0.4±0.7	2.2	3.2	4
Crescent City (CC)	78	0.9±0.2	2.7	3.7	4

Also used are tide gauges listed by *Dragert et al.* [1994].

[a] References: (1) *Hicks* [1978], (2) *Savage et al.* [1991], (3) *Dragert et al.* [1994], and (4) *Mitchell et al.* [1994]. Where different values have been quoted, the reference in parentheses is quoted here.

[b] Actual and projected distances.

[c] Alternative interpretations (see text).

Table 1b. Leveling Data for the Cascadia Margin

Line	Time interval years	Closest Distance From Base of Slope, km	Corrected Uplift of Seaward Point, mm/yr	Uncertainty per 100 km	References [a]
Tofino-Parksville (To-Pa)	12	114	5.0	±0.7	1
Bamfield-Point Alberni (Ba-Pa)	6	122	5.5	±2.0	1
Neah Bay-Twin River	33	160 (projected)	4.0	±1.2	2,3
Twin River-Blyn (Nb-Tr-Bl)	44	193		±0.9	
Westport-Aberdeen	27	135	4.0	±1.5	2
Aberdeen-Olympia (We-Ab-Ol)	55	167		±0.7	
Warrington-Rainer (Wa-Ra)	21	125	3.5	±3.6	2,3
Hebo-Salem (He-Sa)	11	116	1.0	±3.6	2
Newport-Albany [b]	57	117	0.5	±0.7	2,3
(Np-Al)	11	99	1.0	±3.6	
Reedsport-Drain (Re-Dr)	11	90	2.0	±3.6	2,3
Bandon-Coquille	11	66	3.0	±3.6	2,3
Coquille-Dillard (Ba-Co-Di)	56	83		±0.7	
Arcata-Redding (Ar-Rg)	57	113	3.5	±0.7	3

[a] References: (1) *Dragert et al.* [1994], (2) *Reilinger and Adams* [1982], and (3) *Mitchell et al.* [1994].

[b] Two levelings of the line over different time intervals.

the lines with repeat intervals of ~50 years (i.e., those Washington, Oregon and northern California lines with 1987-1988 releveling) to ±3.6 mm/yr for lines with repeat intervals of ~10 years. The observed vertical motions are large compared to the errors for the lines with long repeat intervals but are comparable to the errors for the lines with short repeat intervals. Thus the short-interval surveys provide limited discrimination of the width of the locked zone. The Vancouver Island surveys were to special order requiring maximum misclosures of 3 mm· $K^{1/2}$. The exacting survey standards however resulted in actual leveling errors estimated from forward and backward leveling misclosures that were very much better, about 0.8 mm· $K^{1/2}$ [*Dragert et al.*, 1994]. The latter errors are shown in the Figure 6. The high accuracy of the southern Vancouver Island surveys allowed good resolution of vertical motion even with the short repeat time intervals of 4-12 years between surveys.

The long term trends in tide gauge data allow determination of coastal uplift or subsidence relative to a global sea level reference, but they are subject to a number of nontectonic oceanographic effects such as variations in atmospheric loading, storm surges, El Niño, and other large-scale ocean current and temperature changes. The maximum timescale for most of the larger oceanographic effects is 10-20 years so they can be satisfactorily removed from the long-term trend if the record is for at least 50 years. Taking the tidal level differences compared to well-determined reference stations allows tide gauges with records as short as 20 years to be used. The data have been corrected for present global eustatic sealevel rise of 1.8 mm/yr,

Table 1c. Geodetic Data for the Cascadia Margin From Positional Surveys

Network	Average Distance to Base of Slope km	Shortening Rate μstrain/yr	References [a]
Alberni	160	0.06±0.03	1
Juan de Fuca [b]	180	0.18±0.04	2
Bellingham [c]	280	0.12±0.09	3
Olympic	220	0.09±0.03	4
Seattle	250	0.04±0.01	4
Columbia	160	0.09±0.03	5,6
Portland	220	0.06±0.03	3,6

[a] References: (1) *Dragert et al.* [1994], (2) *Lisowski et al.* [1989], (3) *Snay and Matsikari* [1991], (4) *Savage et al.* [1991], (5) M. Lisowski (personal communication, 1991), and (6) *Vincent* [1989];

[b] Landward decrease in strain rate is just resolved.

[c] Large uncertainty, so not plotted.

Table 1d. Geodetic Data for the Cascadia Margin From GPS

Station	Distance From Base of Slope, km	Horizontal Difference mm/yr	Vertical Difference mm/yr
Penticton (DRAO)	230		
Victoria (ALBH)	520	7.0 [a] ±1.0 [b]	0.6±1.8

[a] Relative to Penticton (DRAO) which is within 1 mm/yr, vertical and horizontal of stable North America.

[b] 95% confidence limit.

the value given by *Douglas* [1991] and *Trupin and Wahr* [1990]. They gave an uncertainty in this rate of ±0.1 mm/yr. The glacial isostatic rebound correction is the same as for the leveling data described above. Numerous tide gauge analyses have been reported [e.g., *Savage et al.*, 1991; *Riddihough*, 1982; *Clague et al.*, 1982; *Holdahl et al.*, 1989]. *Dragert et al.* [1994] presented a summary of the tide gauge data for southern Vancouver Island and northern Washington, and *Mitchell et al.* [1994] presented the data for Oregon and northern California. The more reliable data are listed in Table 1. The Washington, Oregon, and northern California tide gauge data are shown on our model profiles; *Dragert et al.* [1994] have previously compared the southern British Columbia and northern Washington data to dislocation models.

One repeated very high precision gravity survey has been carried out across southern Vancouver Island [*Dragert et al.*, 1994]. The time interval between surveys was only 4 years so the errors in vertical motion are large. However, the gravity changes corrected for postglacial rebound are equivalent to uplift of the outer coast relative to 100 km inland at a rate of about 5 mm/yr. The gravity data thus substantiate the conclusions from the leveling and tide gauges. Absolute gravity surveys now in progress will allow absolute vertical motions to be determined within about 5 years.

Savage et al. [1981] first showed that there was shortening across the margin at a rate similar to that expected for a locked subduction thrust fault. Repeated measurements for seven horizontal strain arrays have been reported for the Cascadia region [*Lisowski et al.*, 1989; *Dragert and Lisowski*, 1990; *Savage et al.*, 1981, 1991; *Snay and Matsikari*, 1991; *Dragert et al.*, 1994]. Most of the surveys indicate shortening approximately perpendicular to the margin. Only the Alberni network has the maximum shortening direction significantly oblique to the margin, as discussed by *Dragert et al.* [1994], and we have used the shortening component resolved in the direction of the model profile. This network is probably affected by the proximity of the northern end of the subduction zone. Where only triangulation data are available, strain must be derived from angle changes, and the amount of shortening is ambiguous; we have assumed that the deformation is uniaxial in the direction of the profiles.

Global Positioning System (GPS) relative positions have been recorded continuously for 2 years at three stations in the region, Victoria (ABHD) on southernmost Vancouver Island, Holberg (HOLB) on northernmost Vancouver Island, and Penticton (DRAO) (just to the east of Figure 1), in south central British Columbia [*Dragert and Hyndman*, 1995]. Penticton is 515 km from the deformation front and is taken to be on stable North America. The motion of Victoria with respect to Penticton is landward in the direction of plate convergence expected for a locked subduction thrust. However, the motion of Holberg, which is in the area of the plate triple junction, is to the northwest, parallel to the margin. It also has rapid uplift. This indicates that simple two-dimensional deformation associated with Cascadia great earthquakes does not extend to northern Vancouver Island.

Elastic Dislocation Models and the Width of the Locked Zone

Elastic Dislocation Models

In this section we compare the observed current deformation to that predicted by simple elastic dislocation models in order to estimate the portion of the subduction thrust fault that is locked and storing elastic strain to be released in future great earthquakes. For modeling the coseismic deformation, the elastic dislocation approach involves prescribing a downdip displacement on the rupture zone, with the fault at greater depth being "locked." For the interseismic deformation, it involves a locked upper seaward part of the fault and a prescribed velocity (i.e., plate convergence rate) on the deep part of the fault. If the steady subduction component is subtracted to allow a net zero displacement through the earthquake cycle, the locked part of the fault has reverse interseismic motion at the plate convergence rate. For either the coseismic or coseismic deformation, the wider the seismic rupture or locked zone, the wider is the surface deformation zone; the pattern of deformation defines the downdip width of the rupture or locked zone.

For the interseismic period, application of this model assumes (1) that the earthquake deformation cycle may be approximated by elastic behavior, (2) that there is no permanent deformation through the earthquake cycle, (3) that the surface deformation is solely a function of the distribution of slip velocity as a function of downdip distance on the subduction thrust fault, and (4) that the slip velocity is a simple prescribed function of depth (to allow model fitting of observed data), i.e., constant velocity below a certain depth, with a transition zone updip to the fully locked zone. To estimate the coseismic rupture zone from the Cascadia interseismic data, it is also necessary to assume that the present surface deformation rate (and thus locked zone)

remains approximately constant with time through the interseismic period.

Such models are an incomplete representation of the complex viscoelastic interaction between the two plates [*Thatcher and Rundle*, 1984; *Wang et al.*, 1994]. Further work is required to understand the deformation through the earthquake cycle and how in detail the interseismic deformation is restricted to the region of the locked fault zone. However, we conclude that purely elastic dislocation models provide a reasonable approximation for definition of the width of the locked seismogenic zone. The nonelastic component of the behavior may be partly accommodated by second-order adjustments to the elastic models, for example, the transient over a few years immediately following a great earthquake. Support that the elastic dislocation model applied to the interseismic deformation data provides a reasonable definition (±15-20%) of the maximum great earthquake rupture zone width is provided by the following observations:

1. A comparison of coseismic and interseismic deformation at other subduction zones shows that the pattern of interseismic deformation is approximately the inverse of that for the coseismic rupture (for the southwest Japan Nankai margin, see *Thatcher* [1984] and *Hyndman et al.* [1995]; for the great 1964 Alaska earthquake see *Savage and Plafker* [1991]; and for the 1960 Chile great earthquake, see *Barrientos and Plafker* [1992]). For the southwest Japan margin where there are the best data, the rates of interseismic deformation (vertical and horizontal) times the great earthquake return period approximately equal the negative of the coseismic deformation for the most recent great events (1944 and 1946) (Figure 4). The agreement is particularly good between the coseismic and mid-interseismic period profiles, the peaks in vertical motion being within a few kilometers. Thus the estimated interseismic locked zone is inferred to closely approximate the maximum coseismic rupture zone. A second-order adjustment to the model allows for the displacement to extend with decreasing offset several tens's of kilometers downdip from the main coseismic rupture zone for a few years following the earthquake, i.e., to account for the larger rates in the immediate postseismic period (Figure 4).

2. For the southwest Japan margin, the landward extent of the locked zone defined by modeling the interseismic (and coseismic) geodetic deformation is in general agreement with the coseismic rupture zone estimated from seismic and tsunami data for the most recent two great earthquakes (1944 and 1946) (see summary by *Hyndman et al.* [1995]).

3. There is agreement between the locked zone defined by thermal modeling and the locked zone from dislocation modeling of the interseismic deformation (for southwest Japan, see *Hyndman et al.* [1995]; for northern Cascadia, see *Hyndman and Wang* [1993]). General agreement is also found from the additional thermal and deformation modeling of this article.

Dip Geometry of the Subduction Thrust

An important factor in both the deformation and thermal models is the dip geometry of the subduction thrust detachment. For five profiles we have estimated the dip for the seaward portions of the thrust from multichannel seismic reflection data and for the deeper portions from Benioff-Wadati seismicity (assumed to be in the uppermost mantle about 5 km below the top of the downgoing plate), from seismic refraction data, and from seismic tomography (Figure 5 and Table 2). Contours of plate depth are given in Figure 3. The dip profile is well constrained for southern British Columbia and Washington but

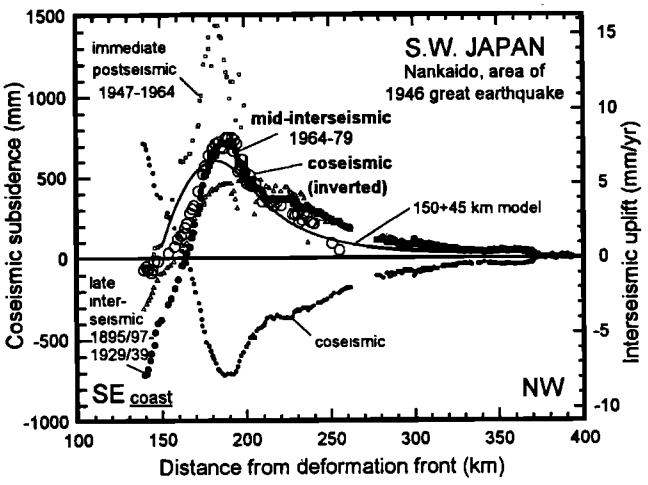

Figure 4. Repeated leveling results across the Nankai margin of southwestern Japan giving the coseismic subsidence (small solid dots), coseismic subsidence inverted (large solid dots), and the interseismic uplift rate for three intervals. The interseismic vertical axis is scaled relative to the coseismic axis by time interval between great earthquakes. Note the agreement in the location of the peaks for the coseismic (inverted) and interseismic profiles, especially for the mid-interseismic period (open circles).

poorly for Oregon where there is almost no Benioff-Wadati seismicity. We illustrate the variation in plate dip parallel to the margin by giving the dip angle at 60 km from the base of the continental slope in Table 2 and text below. We have assumed that the detachment is at the top of the oceanic crust. Seismic reflection data across the frontal thrusts at the base of the continental slope show this to be a good approximation for many of the profiles [e.g., *Davis and Hyndman*, 1989; *Spence et al.*, 1991; *MacKay et al.*, 1992]. However, on some of the seismic sections the detachment is several hundred meters above the oceanic crust, and the lower part of the incoming sediment section is being subducted to some unknown depth. This difference is not important for the deformation models, but it is important for the thermal regime of the seaward portion of the thrust fault. The deformation profiles are described individually below.

Application of Elastic Dislocation Models

For our modeling we have employed the simple dislocation model of a dipping thrust fault in an elastic half space [e.g., *Savage*, 1983]. A transition zone is included between the fully locked and downdip free slip portions of the fault since an abrupt discontinuity is physically unrealistic. Neither the downdip distribution of slip nor the width of the transition zone can be accurately determined from the available deformation data. The model transition has a linear variation of slip rate from completely locked to completely free; more complex model variations in slip are not warranted by the data. The transition widths have been chosen based on the results of the thermal models. For most of the region on land where deformation data are available, there is little difference between the vertical motion model predictions with a transition zone and those for no transition zone but with the fully locked zone extended downdip by half the width of the transition zone. Examples of this trade-off are given by *Dragert et al.* [1994]. The one leveling profile that extends seaward of the peak in uplift, Westport-Olympia, is of low quality but it shows the peak amplitude expected for a

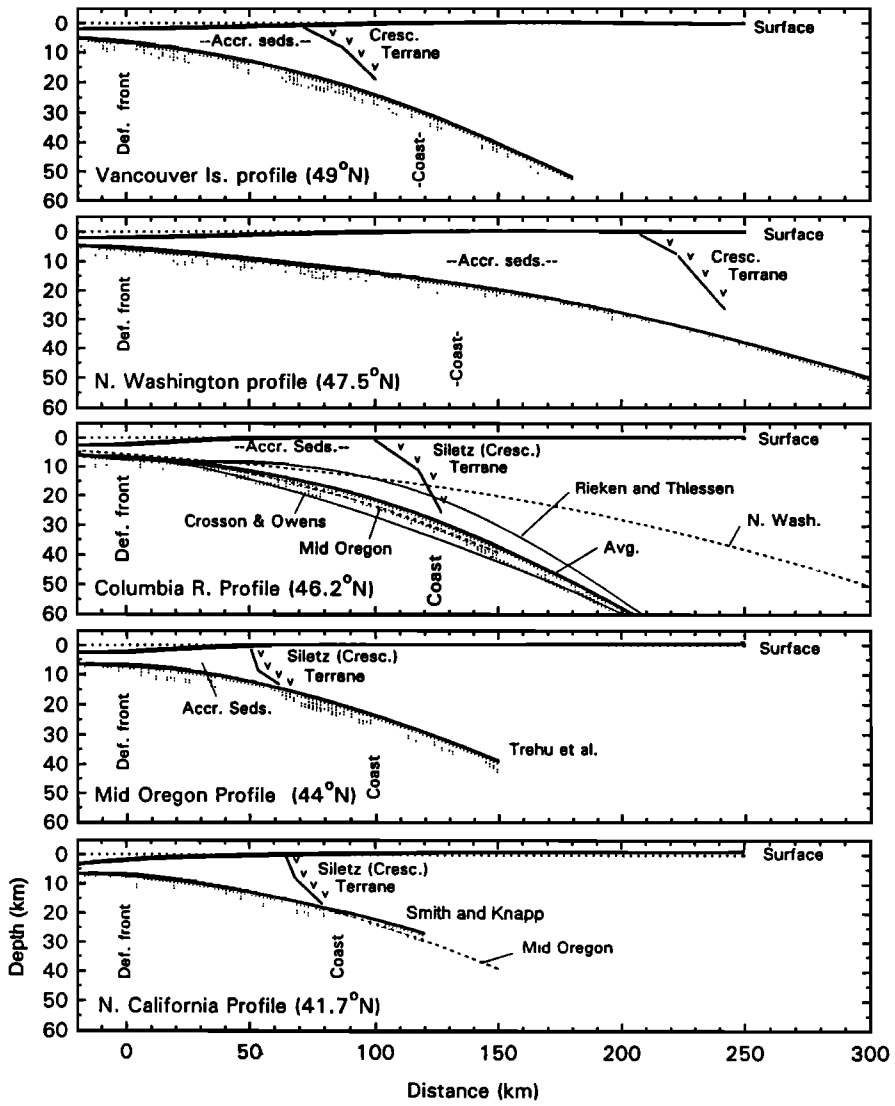

Figure 5. The subduction thrust fault dip geometry for the five Cascadia deformation model profiles. The approximate seaward limits of the Crescent/Siletz basaltic terrane beneath the continental shelf are shown.

transition zone of width comparable to that of the locked zone. For no transition zone, the predicted peak amplitude is about double that observed. Models with little or no transition zone also predict unrealistic oscillations in the spatial variation of the horizontal shortening. Our model has a linear variation of slip within the transition zone. Our model transition zones are in approximate agreement with those obtained from the viscoelastic models of *Wang et al.* [1994].

We have used a single plane fault approximation, asymptotic to the true curved dip profile at the downdip end of the fully locked zone. This is an adequate approximation for predicting deformation in the region on land where geodetic data are available. A more accurate representation is needed to predict the coseismic vertical motion of the continental slope and shelf as involved in tsunami generation. In addition to a more accurate fault geometry, modeling that area over the seaward portion of the accretionary prism must allow for the detailed prism geometry and for a significant part of the plate convergence being accommodated by steady shortening and thickening of the sediment section rather than by elastic shortening and episodic slip on the main subduction thrust.

The elastic dislocation model allows partitioning of the plate convergence into parallel and perpendicular components. Off Washington and Oregon, convergence is about 20° from perpendicular to the margin and we have modeled only the

Table 2. Profile Data

Profile	Ocean Crust Age, m.y.	Basin Sediment Thickness, km	Dip at 60 km, deg
Southern Vancouver Island	7	4.5	12
Northern Washington	8	3.75	5
Columbia River	8.5	3.5	9
Mid-Oregon	8.5	3.5	11
Northern California [a]	~6	2.7	9-10

[a] Large uncertainty in age, convergence rate, etc., so results not presented.

perpendicular component. The present convergence rates along the Cascadia margin as estimated by *Riddihough* [1984] decrease slightly to the south from 47 to 37 mm/yr from southern Vancouver Island (south of Nootka Fault) to Cape Blanco off southern Oregon. *DeMets et al.* [1990] estimated a slightly slower present convergence rate of 42 mm/yr and a more clockwise (N69°E) convergence direction for the Washington margin. The convergence rate off southernmost Oregon and northern California is not well constrained since the oceanic plate appears to be breaking up and the tectonic regime is complex [e.g., *Riddihough*, 1980; *Wilson*, 1989]. The convergence rate in this region may decrease rapidly to the south toward the triple junction. Our conclusions are not sensitive to a rate variation between 30 and 50 mm/yr, and we have used an orthogonal component rate of 40 mm/yr for all of the models. Different convergence rates change only the deformation magnitudes not their spatial form. We have not attempted to model the three-dimensional effects at the north and south ends of the subduction zone. The bend in the margin at the Strait of Juan de Fuca and Olympic Peninsula involves a change in strike over distances that are greater than the downdip width of the locked zone. Thus, although this corner results in a large variation in plate dip along the margin, we expect two-dimensional models to be an adequate approximation. Our study for the southwest Japan subduction zone [*Hyndman et al.*, 1995] showed that two-dimensional models give reasonable results near a much sharper corner, which supports this conclusion.

We have employed five model cross sections that should adequately represent the variations in deformation and thermal parameters parallel to the Cascadia margin (Figure 3). An additional deformation model profile has been presented by *Dragert and Hyndman* [1995] through the northern Olympic Peninsula of Washington and southernmost Vancouver Island. We present the predicted deformation for three widths of locked and transition zones for comparison with the different deformation data sets. The model widths of 40 km locked plus 40 km transition, 60 km plus 60 km, and 100 km plus 100 km represent the range of inferred widths for different portions of the margin. More precise fits of models to the data were employed to give the model locked zone widths shown in Figure 1. The results for the nearest model profile are used for comparison with the deformation data. The available data do not warrant inversion of the geodetic data for the fault slip distribution [e.g., *Arnadottir et al.*, 1992].

Deformation Data

We present the repeated leveling data for 10 lines that are approximately perpendicular to the margin (locations in Figure 3) for comparison with the model predictions of the nearest of the profiles. The tide gauge data are plotted with the nearest leveling results We also present the linked leveling line data for lines generally along the coast from Mitchell et al. [1994].

Southern Vancouver Island profile. The data from two leveling lines, from the long term trends in tide gauge records, and from repeated precision gravity for this profile have been discussed by *Dragert et al.* [1994] and *Hyndman and Wang* [1993]. The fault dip profile (Figure 5) is well constrained by multichannel seismic reflection data for the offshore and western Vancouver Island portion, and by Benioff-Wadati seismicity and seismic refraction beneath Vancouver Island [e.g., *Hyndman et al.*, 1990]. Farther inland the position of the plate is constrained by teleseismic data [*Cassidy and Ellis*, 1993; *Bostock and VanDecar*, 1995; *Cassidy*, 1995]. The dip at a distance of 60 km from the base of the continental slope is 12°. At the deformation front (base of the continental slope) the detachment is close to the top of the oceanic crust [*Davis and Hyndman*, 1989; *Spence et al.*, 1991; *Hyndman et al.*, 1994]. We compare the leveling data from two lines, Tofino-Parksville (To-Pa) and Bamfield-Port Alberni (Ba-Al) (the Tofino-Parksville line has two repeated surveys) [*Dragert et al.*, 1994], to the dislocation model predictions in Figures 6a and 6b. We have not presented the repeated gravity data (located along the Tofino-Parksville leveling line); they have much lower accuracy and have been compared to dislocation models by *Dragert et al.* [1994]. They show a similar pattern to the leveling, although with a somewhat greater uplift rate [*Dragert et al.*, 1994]. All of the vertical data fit the 60 km locked plus 60 km transition model best. The Tofino-Parksville line extends slightly closer to the base of the continental slope than the Bamfield-Port Alberni line, and it fits slightly narrower widths. For both lines, model widths narrower than 50 + 50 km and wider than 70 + 70 km appear to be excluded.

The horizontal shortening data for the Alberni network on southern Vancouver Island [*Dragert et al.*, 1994; *Lisowski et al.*, 1989] are compared to dislocation model predictions in Figure 8a. As noted above, this network indicates oblique shortening and the value resolved in the direction of the profile is plotted. The positional results are in agreement with the predictions of the 60 plus 60 km model; they just exclude the 40 plus 40 km model but not the 100 plus 100 km model.

Northern Washington (Olympic) profile. This model profile crosses the margin where plate dip is shallowest and thus the locked zone is expected to be the widest. The dip profile (Figure 5) is well constrained by offshore multichannel seismic reflection data across the lower slope [*Snavely and Wagner*, 1981; *Snavely*, 1987; *Spence et al.*, 1991] and Benioff-Wadati seismicity farther landward [*Crosson and Owens*, 1987; *Rieken and Thiessen*, 1992]. Teleseismic wave modeling also provides constraint for the deeper portion of the subducted slab [*Crosson and Owens*, 1987; *Owens et al.*, 1988; *Rasmussen and Hymphreys*, 1988; *Bostock and VanDecar*, 1995]. The dip at 60 km landward of the base of the slope is very shallow, about 5°. Quantitative interpretation of the models must be treated with some caution because of our use of a two-dimensional model in a region of a three-dimensional corner in the margin. Two leveling lines are available, one north and one south of the model profile. There are also two tide gauges and a continuous recording GPS site.

The repeated leveling line along the north coast of the Olympic Peninsula, Neah Bay - Twin River - Blyn (Nb-Tr-Bl) [e.g., *Reilinger and Adams*, 1982] (Figure 3) is at an angle of about 40° to the trend of the outer coast and to the profile. The leveling data have been projected onto the profile. The repeated surveys are over long time intervals and the estimated errors are sufficiently small for the vertical motion to be well resolved. There are two independent line segments (Neah Bay - Twin River, with a repeat interval of 33 years; Twin River - Blyn, with a repeat interval of 44 years), and we have adjusted their absolute levels so that they approximately align at their adjacent ends. We have accumulated the error estimates for the combined lines (Figure 6c) (see also *Dragert et al.* [1994]). We also show the vertical motion curve obtained by *Ando and Balazs* [1979] from lines around the Olympic Peninsula and Puget Sound that include the line that we present. We have projected their curve onto the northern Washington model profile

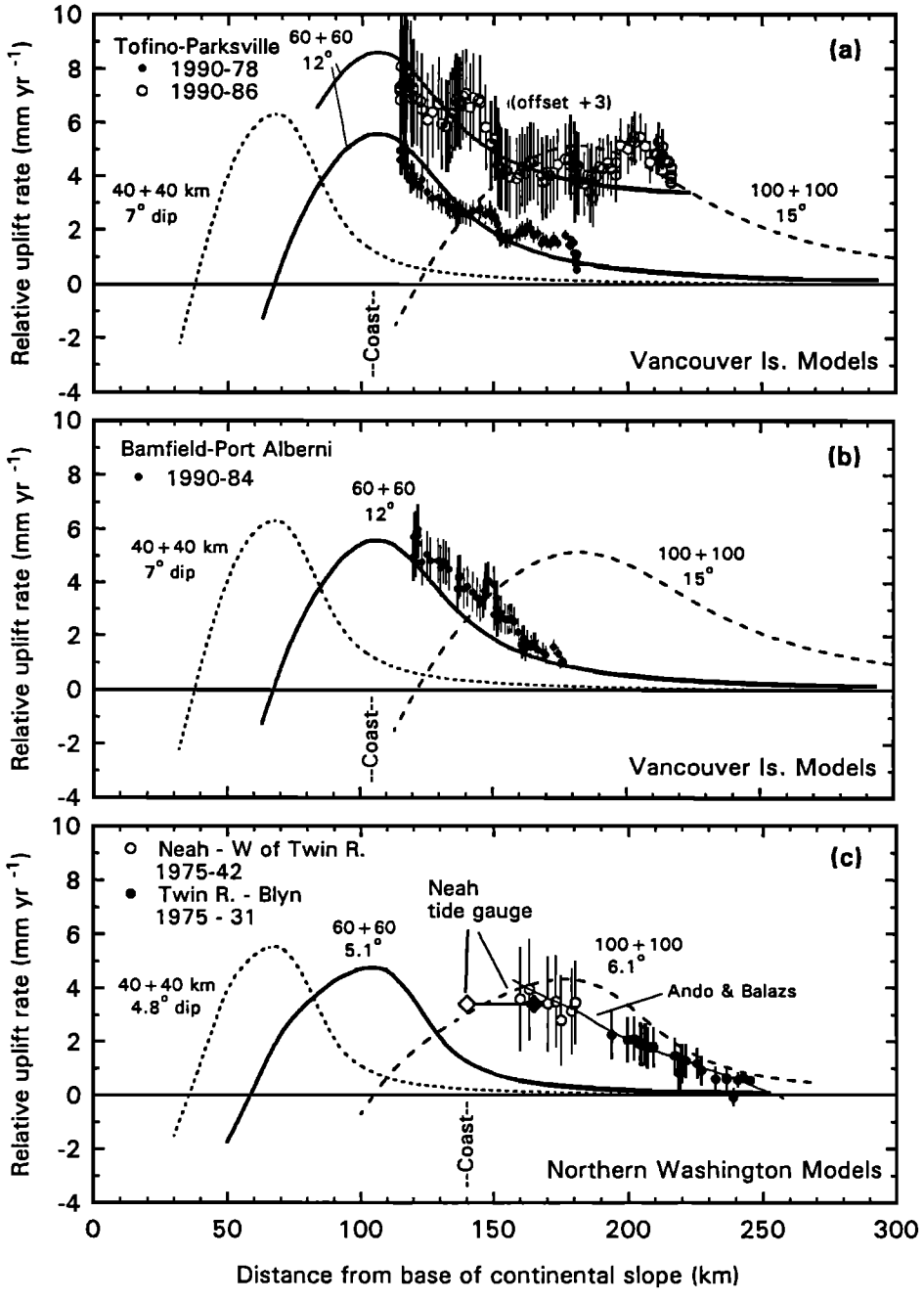

Figure 6. Profiles of current vertical motion across the Cascadia margin from repeated leveling lines and tide gauge data. The leveling line error bars illustrate the estimated propagation of uncertainty with survey distance, the inland ends being taken fixed. They are not uncertainties on individual points. The data are compared to the predictions of elastic dislocation models with three combinations of widths of locked and transition zones, 40 km locked plus 40 km transition, 60 and 60 km, and 100 and 100 km. The Neah Bay-Twin River-Blyn (Olympic Peninsula) data (Figure 6c) have been projected onto a line perpendicular to the trend of the base of the continental slope. The projected (solid symbol) and actual unprojected distance (open circle) to the base of the continental slope for the Neah Bay tide gauge are shown. The two alternative interpretations for the Toke Point (TP) tide gauge are shown for the Westport-Aberdeen-Olympia (northern Washington) line (Figure 6d). The solid symbol is our preferred interpretation. Several lines have two independent segments that have been approximately aligned at their adjacent ends. The four open circles for the Hebo-Salem (He-Sa) line are taken to unreliable. The dip angles given are at the downdip end of the model locked zones. There data for two time intervals on the Tofino (To) and Newport Albany (Np-Al) lines. The data for one interval and the model that agrees most closely have been vertically offset for clarity.

(perpendicular to margin) and corrected it for postglacial rebound following *Dragert et al.* [1994]. Both the projection and the postglacial rebound correction steepen the curve. The best model agreement for all of the leveling data is for 90 km locked and 90 km transition zone.

The results for the Neah Bay (NB) tide gauge located at the seaward end of the leveling line are plotted both at the actual distance from the base of the continental slope and at the distance from projection onto the model profile. The projected tide gauge point gives good general agreement to the 100 + 100

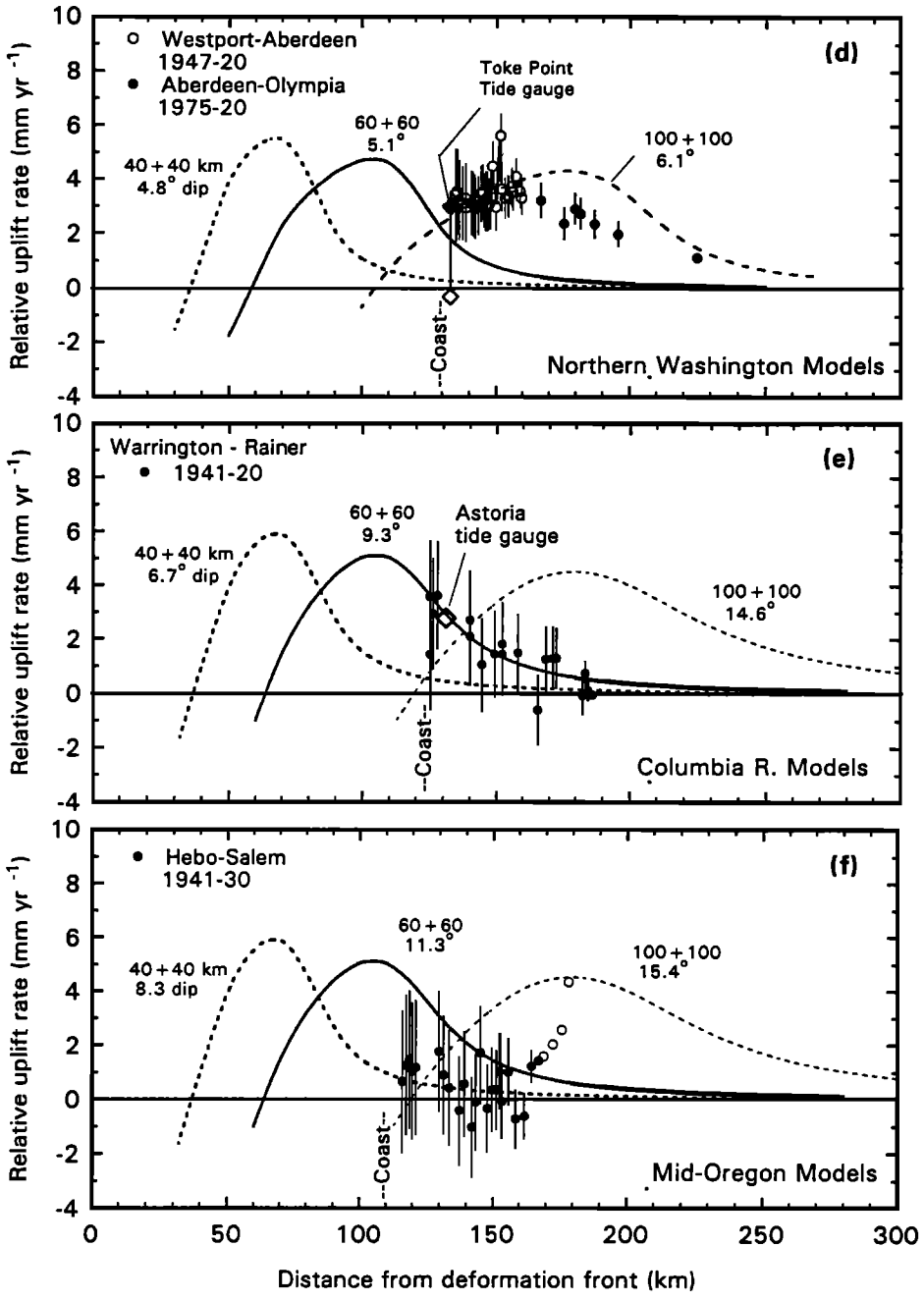

Figure 6. (continued)

km model as previously shown by *Savage et al.* [1991] and *Dragert et al.* [1994]. The point plotted at its actual location between the Vancouver Island and northern Washington profiles fits either the 60 + 60 km or the 100 + 100 km models. The continuous GPS recording station at Victoria (ALBH) [*Dragert and Hyndman,* 1995] lies to the north of the model profile, but it is located where the plate dip is only slightly less than that for the northern Washington profile (Figure 3). The uncertainty in the vertical GPS data is too large to provide significant model constraint, but there is agreement with either the 60 + 60 km or 100 + 100 km models.

The second leveling line also has data for two unconnected segments, Westport - Raymond, (27 years) and Aberdeen - Olympia (54 years) (We-Ab-Ol) [e.g., *Reilinger and Adams,* 1982] (Figure 6d). The two segments have been approximately aligned at their adjacent ends. The best agreement is again for slightly narrower than the 100 + 100 km model. The recording duration of the Toke Point (TP) tide gauge is too short to allow strong model constraint. By taking the relative levels with respect to the Neah Bay (NB) and to the Astoria (AS) tide gauges, *Mitchell et al.* [1994] interpreted near zero vertical motion. This result seems inconsistent with the leveling data which gives coastal uplift of at least 2 mm/yr relative to further inland and little tilt along the line north to Neah Bay in the original along-coast leveling data [*Ando and Balazs,* 1979]. The *Mitchell et al.* [1994] interpretation also requires a rapid change in uplift parallel to the margin from Toke Point to Astoria located only 80 km to the south. Such a rapid change is physically unlikely based on our dislocation models. A zero uplift rate is also in disagreement with the shortening observed

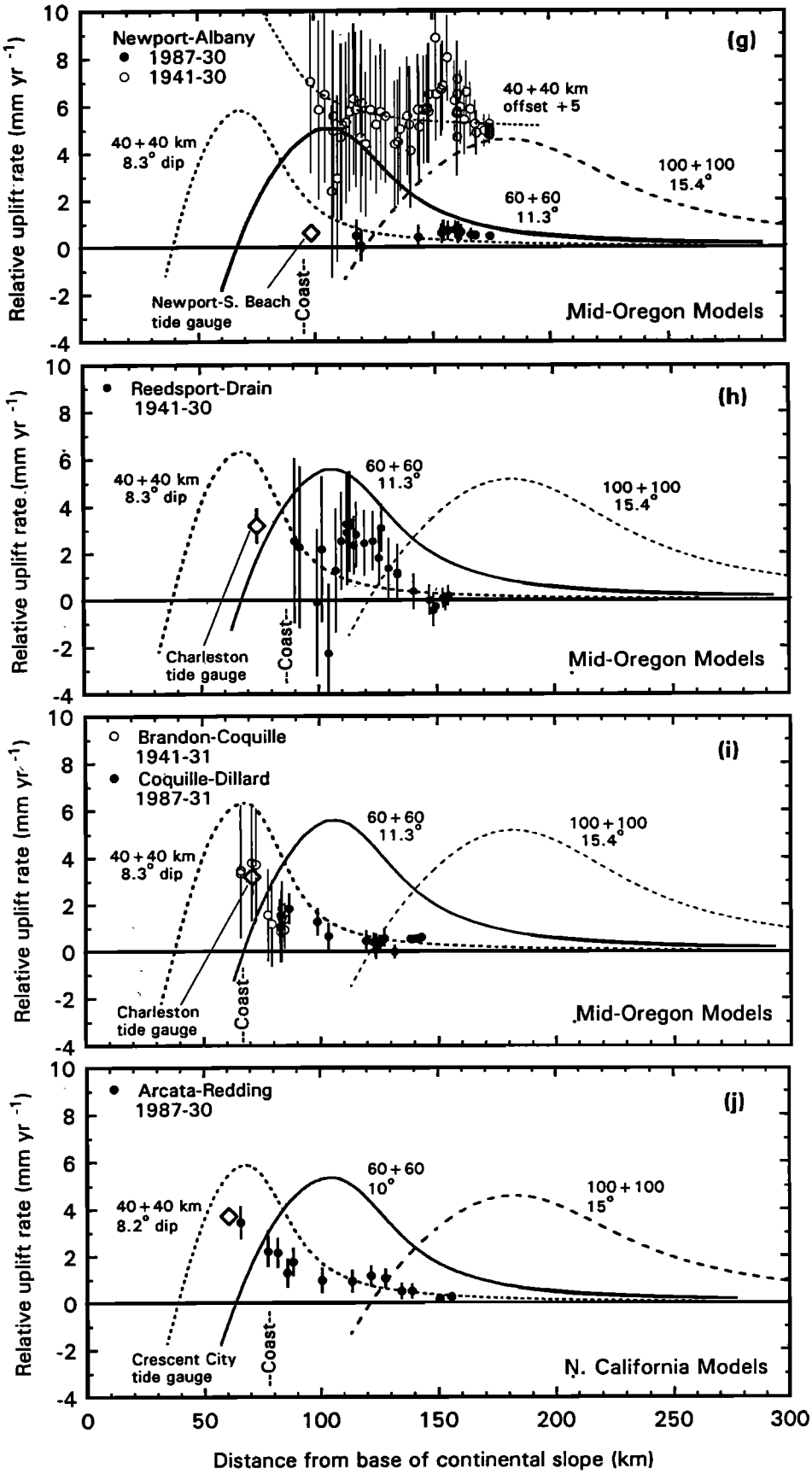

Figure 6. (continued)

inland at the Seattle network and with our thermally estimated locked zone. However, if the first few years of intermittent Toke Point data are excluded (Figure 7), the trends relative to both Neah Bay and Astoria give uplift at Toke Point of 3-3.5 mm/yr. We prefer this interpretation and use it in our analysis but recognize the large uncertainty.

Four horizontal networks provide data associated with this profile (Juan de Fuca, Olympic, Seattle and Bellingham) [*Dragert et al.*, 1994; *Savage et al.*, 1981, 1991; *Snay and Matsikari*, 1991; *Lisowski et al.*, 1989]. The Bellingham network result is in agreement with the adjacent Seattle network data but has errors that are too large to provide additional constraint. The other three network results are in agreement with the 100 km locked and 100 km transition zone model or slightly narrower; the 60+60 km and narrower models appear to be excluded (Figure 8b). The Juan de Fuca network covers enough distance perpendicular to the margin to just resolve a landward decrease in horizontal shortening rate as predicted by the models. The continuous GPS data give a landward motion of Victoria (ALBH) with respect to the reference station Penticton (DRAO) of 7 mm/yr [*Dragert and Hyndman*, 1995] (Table 1). The best fit for these data is to the model with 100 + 100 km locked and transition zones (Figure 9).

Columbia River profile. There is poor control on the plate dip for this profile (Figure 5). The location is just beyond the southern limit of significant Benioff-Wadati seismicity and we have taken an average of the seismicity depth contours by *Crosson and Owens* [1987] and by *Rieken and Thiessen* [1992]. This average gives a similar dip profile to that from seismic refraction at the mid-Oregon profile to the south. The estimated plate dip at a distance of 60 km from the base of continental slope is 9°. The leveling data, Warrington - Rainier (Wa-Ra) (21 years) along the Columbia River perpendicular to the coast, have moderately large error estimates, but they still provide strong constraint to the 60 + 60 km model (Figure 6e).

The Astoria (AS) tide gauge provides good control at the seaward end of the leveling line, and its data also constrain the model to 60 km locked plus 60 km transition (Figure 6e). The tide gauge station is located at the mouth of the Columbia River and the levels have been affected by a change in seasonal river flow resulting from the building of a series of dams on the river

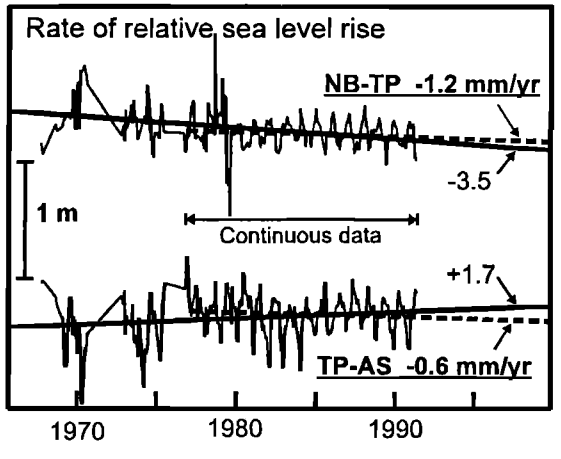

Figure 7. Vertical motion of the Toke Point (TP) tide gauge as a function of time with respect to the Neah Bay (NB) and Astoria (AS) stations (modified from *Mitchell et al.* [1994]). The dashed lines and the underlined values are the proposed revisions using only the period of continuous data; the solid lines and other values are the original interpretation.

over the past 50 years. However, *Mitchell et al.* [1994] provided a correction for this effect. *Mitchell et al.* [1994] also present data for the Garibaldi tide gauge 70 km to the south of Astoria, but the recording duration is too short for the data to provide useful model constraint.

Two horizontal positional networks provide data for this profile, the Columbia network in the region of the lower Columbia River (Figure 8c) (M. Lisowski, personal communication, 1991) and the Portland network [*Snay and Matsikari*, 1991]. They give agreement with either the 100 + 100 km or the 60 + 60 km models but exclude the 40 + 40 km model.

Mid-Oregon profile. There is almost no Benioff-Wadati seismicity to define the plate dip in the region of this profile. Constraint is provided by multichannel seismic reflection data for under the continental slope and by seismic refraction for under the shelf [*MacKay et al.*, 1992; *Trehu et al.*, 1995a, b], although the latter does not have good resolution of the downgoing plate beneath the coast. The seismic tomography of *Rasmussen and Hymphreys* [1988] farther inland substantiates that the plate dips more steeply than to the north. The estimated dip at 60 km is 11°. The model profile has been used for comparison with the results from four leveling lines, Hebo - Salem (He-Sa, 11 years), Newport - Albany (Np-Al, 57 years), Reedsport-Drain (Re-Dr, 11 years), and Bandon - Coquille - Dillard (Ba-Co-Wd, 56 years).

The trend for the Hebo - Salem line (Figure 6f) has almost no relative vertical motion between the ends of the line as expected for model locked and transition zones of 40 km + 40 km or narrower. However, the error estimates are too large to allow strong model control. The rapid uplift at the landward end of this line (shown by open circles) is unlikely to be associated with the great earthquake cycle; it may result from groundwater processes in the sediments of the Willamette Valley. The Newport-Albany line (Figure 6g) has excellent data with repeated leveling in 1987, 1941 and 1930. The results for the two time intervals are in good agreement. The longer time interval allows strong constraint on the model; the best fit is for a 35 km locked and 35 km transition zones or narrower. Wider zones are excluded. The Reedsport to Drain line (Figure 6h) again best fits the 40 + 40 km model, but it has large estimated errors so does not provide strong constraint. The Bandon-Coquille-Dillard line (Figure 6i) has two segments that have been approximately aligned. The estimated errors are sufficiently small that they allow good constraint to a 35 + 35 km model. Wider and narrower models are excluded. The small rate of uplift at the coast for the central Oregon region is clear in the north-south coastal leveling line [*Mitchell et al.*, 1994] (Figure 10). There is a dip in the repeated leveling results in central Oregon of about 2 mm/yr relative to the areas to the north and to the south.

The Newport/South Beach tide gauge (NP/SB) has quite good data and also constrains the model to be about 35 + 35 km (Figure 6g). The Charleston tide gauge (CH) is located between the Reedsport to Drain line and the Bandon-Coquille-Dillard line. The data are of only fair quality (differenced to South Beach) but give good confirmation of widths of about 35 + 35 km. The Port Orford tide gauge data [*Mitchell et al.*, 1994] have uncertainties that are too large for the data to be useful.

There are no horizontal positioning network data available in the area of this model profile.

Northern California profile. There is substantial seismicity near the triple junction at the south end of the subduction zone [*Smith and Knapp*, 1993], although there is uncertainty as to

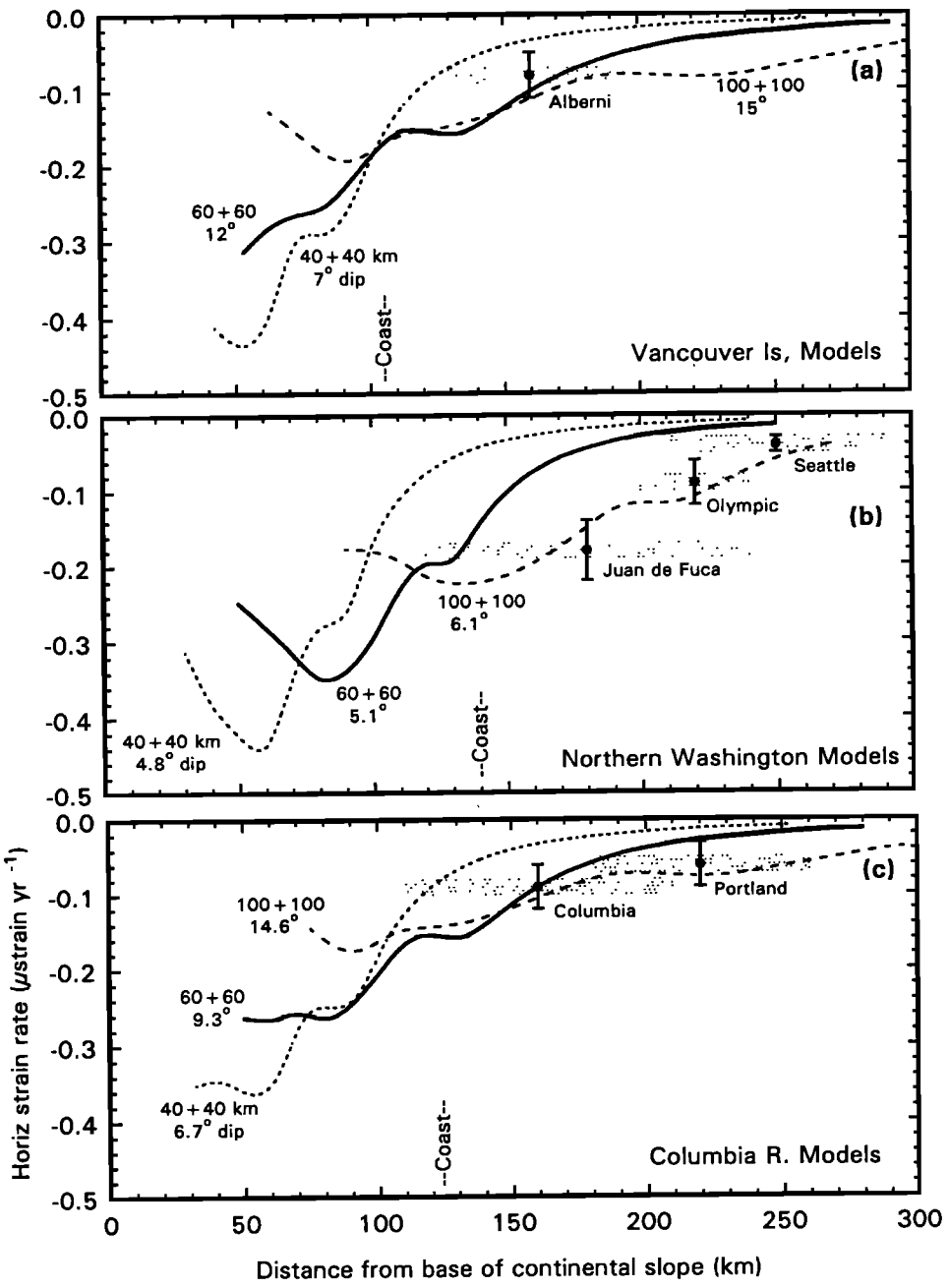

Figure 8. Horizontal strain rate measurements compared to the predictions of elastic dislocation models with three combinations of widths of locked and transition zones. The vertical and horizontal bounds shown are the strain rate uncertainties and the network extents.

which earthquakes are on the subduction thrust plane and which are Benioff-Wadati earthquakes within the oceanic plate. We have taken the interpretation of *Wang and Rogers* [1994] which gives a dip of 9-10° at 60 km from the deformation front. This is slightly shallower than for the mid-Oregon profile. The Arcata to Redding line (Ar-Rg) provides good data that constrain the model to widths of about 40 + 40 km (Figure 6j). However, these data must be interpreted with caution because the line is close to the southern end of the subduction zone and because the breakup of the Gorda plate results in complex tectonics with poorly known convergence rate and direction. The Crescent City (CC) tide gauge located about 75 km to the north provided good data that fit the 40 + 40 km model, and exclude much narrower and wider models.

There are no horizontal positioning networks available that are applicable to this model profile.

Summary of Deformation Constraints

The 10 leveling lines and the tide gauge data all exhibit uplift of the coast; the rate is ~4 mm/yr with the exception of central Oregon where it is ~1 mm/yr. This variation along the coast is supported by coast-parallel leveling lines [*Mitchell et al.*, 1994] (Figure 10) which show a low in relative uplift rate along the coast of Oregon. It is noted that some of the rapid variations, over ~100 km distances, along these coast-parallel lines is because sections run inland or follow sharp irregularities in the coastline. Shortening across the horizontal position arrays that lie near the coast is approximately perpendicular to the margin

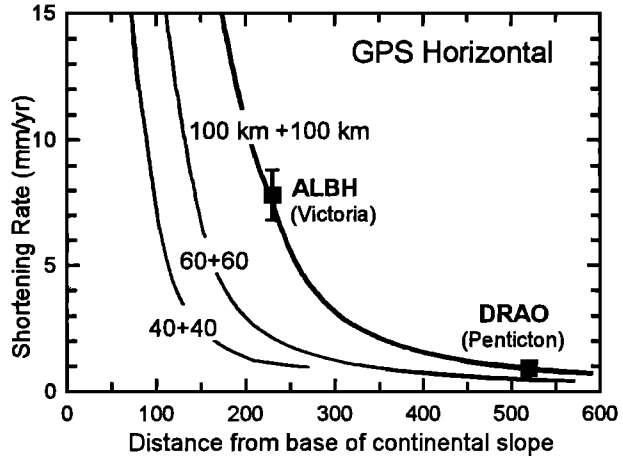

Figure 9. The horizontal landward motion of the Victoria (ALBH) GPS station with respect to the inland Penticton (DRAO) station which is nearly fixed relative to stable North America. The results are compared to model curves with several widths of locked and transition zones.

(except as noted for Alberni) at rates of ~0.1 μstrain/yr. The networks farther inland (Bellingham, Seattle, Portland) exhibit smaller strain rates as expected for a locked zone that lies seaward of the coast. The southern Vancouver Island GPS data indicate landward motion of the coastal zone relative to stable North America (taken as Penticton DRAO site) of 7 mm/yr, about 20% of the plate convergence rate. The GPS data provide a particularly important model constraint since they give the horizontal displacement rate relative to stable North America, rather than just the local strain rate. The best fit to the model widths for all of the vertical and horizontal data follows the plate dip. It is about 60 + 60 km along the margin of Vancouver Island. It widens to about 90 + 90 km at the Olympic Peninsula of northern Washington where the plate dip shallows. The widths narrow to about 35+35 km off Oregon and northern California where the dip is steeper. The better geodetic data provide quite precise constraint to the dislocation models, generally within ±10 km for the model locked and transition zone widths.

In Figure 11 we show contours of present uplift rate for the Cascadia margin using the best fitting elastic dislocation models for all of the geodetic data. The contours are an interpolation based on the assumption, supported by the thermal constraint, that the downdip extent of the locked zone should vary smoothly along the margin. The peak uplift is near the coast, located just onshore for northern Washington, and just offshore for central Oregon. The pattern for the central portion of the Cascadia margin is similar to that given by *Mitchell et al.* [1994] based on leveling data without the additional constraint of the dislocation model assumption, although their pattern shows somewhat greater variability. Our main proposed revision to their pattern is that we tentatively interpret the central Washington leveling and tide gauge data as indicating substantial coastal uplift. The landward limit of the model locked zone corresponds approximately to the seaward 2 mm/yr contour and the landward limit of the transition zone to the landward 2 mm/yr contour. We have not plotted the model subsidence contours seaward of the zero line because there is no data constraint and our models are a poor approximation in that area.

Comparison of Current Uplift and Coseismic Subsidence from Coastal Data

The contours of current uplift (Figure 11) may be used to estimate the coseismic subsidence in great earthquakes. The pattern of coseismic subsidence is particularly important for modeling tsunami wave generation. The abrupt coseismic subsidence from the accumulated uplift, estimated from current geodetic data, may be compared to that from buried coastal marsh data. This is an important direction for further study, and we give only a brief outline here.

The coseismic subsidence may be estimated from current deformation with three assumptions, that the net vertical displacement over a great earthquake cycle (coseismic plus interseismic) is zero, that the interseismic uplift rate is constant over time (see discussion above), and that the most recent great earthquake released all of the elastic strain accumulated as a result of plate convergence in the preceding interseismic period. The expected coseismic subsidence then equals the uplift rate times the interseismic period. The interval between the last two earthquakes, 300 and 690 years ago estimated from deep sea turbidite data [*Adams*, 1990], is about 390 years. There is some evidence for the 690 year event in the coastal marsh data [e.g., *Clague and Bobrowsky*, 1994a, b], but it is absent at most sites [e.g., *Atwater* 1990]. The second most recent event in the coastal data that is well recorded occurred over 900 years ago.

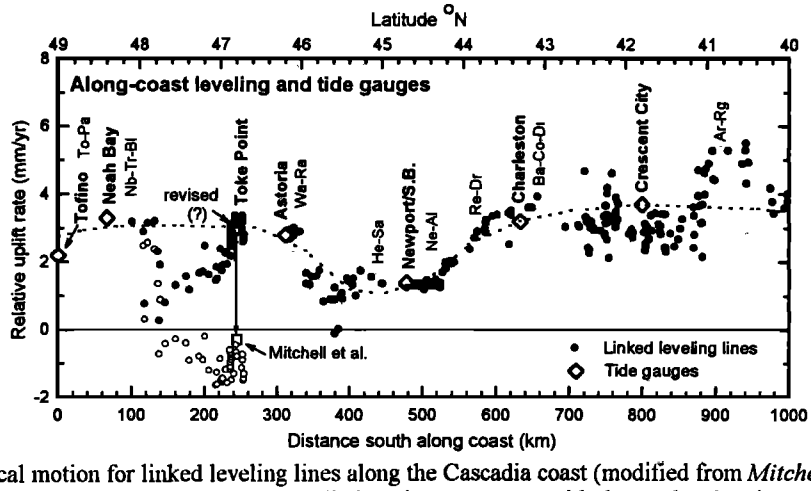

Figure 10. Relative vertical motion for linked leveling lines along the Cascadia coast (modified from *Mitchell et al.* [1994]). A north-south tilt adjustment that is linear with distance has been applied to give agreement with the sea level and postglacial rebound tide gauge data. The original interpretations of *Mitchell et al.* [1994] and our suggested revisions are shown for the Toke Point (TP) tide gauge data and the leveling line linking it to Neah Bay (NB) to the north.

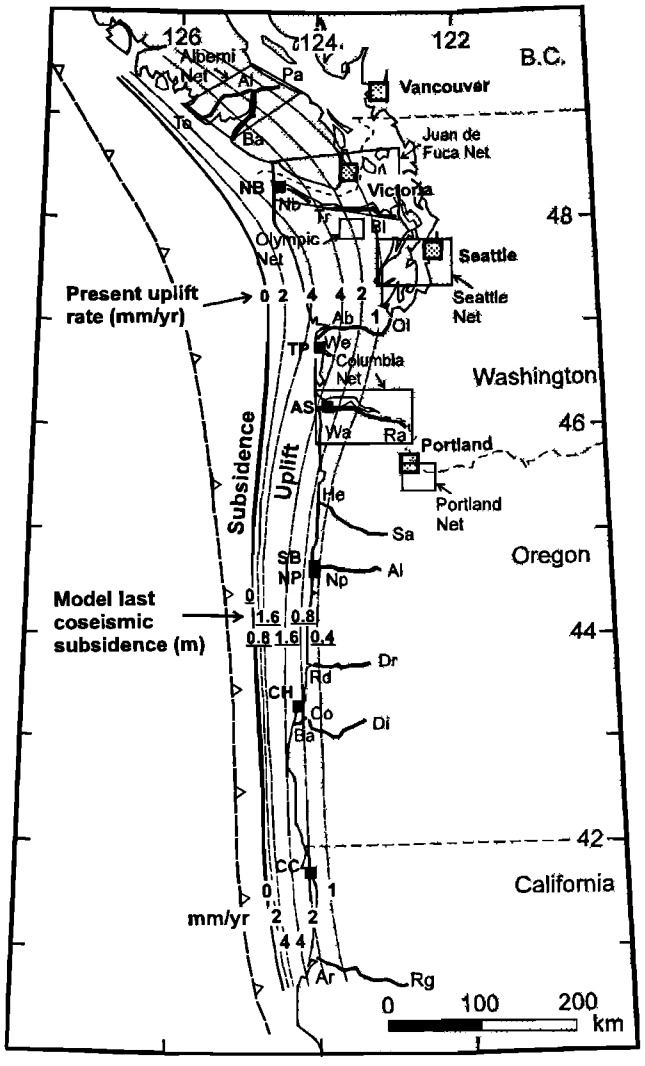

Figure 11. Contours of present uplift rate along the Cascadia margin based on the best fitting elastic dislocation models to the leveling, tide gauge, gravity and positional data. The symbols and abbreviations are as in Figure 3. The model coseismic subsidence (underlined) is given for comparison with paleoseismicity data; it is based on an interval between the last two great earthquakes of 390 years.

Thus the elastic strain release may represent that accumulated over a longer period. For much of the Cascadia outer coast the present uplift rate is about 4 mm/yr so the total interseismic uplift and thus the predicted coseismic subsidence for the last event is 1.6 m assuming a 390-year interval (3.6 m for a 900-year interseismic period). For the coast of central Oregon where the present uplift rate is about 1 mm/yr, the coseismic subsidence estimate is 0.4 m for a 390-year interval.

Coastal intertidal marsh studies from southern Vancouver Island to northern California have found successive buried marsh surfaces (buried peat layers) at increasing depths below the present marsh surface. The paleosurfaces are inferred to result from the abrupt subsidence in great earthquakes, the last 300 years ago [e.g., *Atwater*, 1990]. Three corrections must be applied to the coseismic subsidence estimates from current deformation for comparison with the depth interval between the present coastal marsh surface (present sealevel) and the previous marsh top (preevent sea level): (1) earthquake cycle interseismic uplift since the last event, (2) global eustatic sea level rise since the last event, and (3) postglacial rebound since the last event. For southern Vancouver Island and northern Washington the correction for the interseismic uplift in the 300 years since the last event, at 4 mm/yr, is -1.20 m. For Oregon, at 1 mm/yr, the correction is -0.3 m. During the 300 year period sea level has also risen at a rate of 1.8 mm/yr, i.e., +0.54 m, assuming the same rate as for the present. The postglacial rebound is estimated to be -0.5 mm/yr for southern Vancouver Island, i.e., -0.15 m since the last event. It is about 0 mm/yr for northern Washington, i.e., 0 m since the last event, and +1 mm/yr for Oregon, i.e., +0.3 m since the last event. The total predicted difference between the present marsh level and that just prior to the last event is thus 0.7 m for southern Vancouver Island, 1.2 m for northern Washington, and 0.9 m for Oregon.

Most of the observed depths of the buried coastal intertidal marsh surfaces below the present marsh surface are in the range of 0.3 to 1.2 m for different areas (summary of coastal paleoseismicity data by *Atwater et al.* [1995, and references therein]. The largest predicted and observed depths of the first buried marsh are both for Washington. Although our predicted values are somewhat greater than the observed, the agreements are generally to within about 0.4 m. We consider this to be good correspondence considering the assumptions in our calculation, i.e., that the last great earthquake 300 years ago released exactly the elastic strain built up during the previous interseismic interval (taken to be 390 years) and that the present coastal uplift rates have been constant since the last event. The uncertainties in the corrections discussed above, especially in postglacial rebound, also introduce an uncertainty of at least 0.4 m. We note that the previous interpretation of near-zero present uplift for southern Washington (Toke Point tide gauge) is used [*Mitchell et al.*, 1994], there is a large discrepancy with the buried marsh data for this area.

The immediate coseismic subsidence associated with seismic rupture may be somewhat less than the values based on present uplift rate. Part of the fault slip occurs as postseismic creep on the deeper part of the fault in the period of days to a few tens of years following great earthquakes. Based on observations from southwest Japan, Alaska, and Chile, the immediate peak in coseismic subsidence is located slightly farther seaward than the peak in interseismic uplift. A new approach that allows estimation of the coseismic subsidence is the analysis of foraminifera paleoenvironment and other estimators of water depth before and after great earthquakes. *Guibault et al.* [1994] estimated about 0.7 m of subsidence for the event 300 years ago on the south coast of Vancouver Island which is very close to that estimated from the current uplift.

It is important to recognize that an entire earthquake cycle probably has near-zero vertical displacement. Older intertidal marsh surfaces are preserved at successively greater depths mainly because of sea level rise (plus or minus postglacial recovery). The depth spacing between successive marsh tops is primarily related to the time between the events (i.e., amount of sealevel rise), not to the magnitudes of successive coseismic subsidence.

Thermal Constraints to the Seismogenic Zone

Earthquake Temperature Limits

In this section we estimate the variation in locked zone width along the Cascadia margin from thermal constraints. A number of authors have suggested that temperature may be the primary

constraint on the downdip extent of the locked zone [e.g., *Tichelaar and Ruff*, 1993; *Savage et al.*, 1991; *Hyndman and Wang*, 1993]. Certainly at some depth a temperature is reached where rocks exhibit ductile or plastic behavior and no earthquakes can occur. The critical transition is actually that from seismogenic velocity-weakening to stable-sliding velocity-strengthening behavior [e.g., *Scholtz*, 1990]. Both laboratory data for crustal rocks and the observed maximum depth for crustal earthquakes indicate that the critical temperature is about 350°C (see discussion by *Hyndman and Wang* [1993]). An abrupt discontinuity is physically unrealistic, and there must be a transition zone between where the fault is fully locked and where there is completely free slip, and over which great earthquake rupture decreases to zero. We follow *Hyndman and Wang* [1993] and take the downdip limit of the transition zone to be where the temperature reaches 450°C. This is the temperature for the onset of feldspar plasticity, and the temperature above which there is a rapid increase in instantaneous shear stress. This temperature thus should be the limit of great earthquake fault slip for failure initiated at lower temperature. The two temperatures have considerable uncertainty, both in the best average values and in the variability associated with different rock types and conditions on the fault. Based on the available laboratory and field data, we estimate the 350°C maximum temperature for earthquake initiation in Cascadia to have an uncertainty of ±25°C. The uncertainty of the transition zone temperature limit is probably greater. It is important to recognize that the critical temperature limit for earthquake behavior in the more mafic rocks of the mantle is much higher than 350°C, 750-800°C for most Benioff-Wadati seismicity.

There also may be an updip limit to subduction thrust earthquakes [e.g., *Byrne et al.*, 1988] that is temperature controlled. There may be a minimum temperature for earthquakes defined by where stable-sliding clays are present, such as for accretionary sedimentary prisms [e.g., *Wang*, 1980; *Vrolijk*, 1990]. Such clays dehydrate at 100-150°C to illite and chlorite which are probably seismogenic. For the Cascadia subduction zone, the temperature on the thrust plane at the top of the oceanic crust is ~250°C at the deformation front even before underthrusting starts. Thus no such aseismic zone is expected [*Hyndman and Wang*, 1993]. In contrast, we concluded in our study of the southwestern Japan margin where temperatures are lower, that there is a ~30 km aseismic zone at the updip end of the subduction thrust fault [*Hyndman et al.*, 1995]. The updip limit to the seismogenic zone remains an important uncertainty, especially for models of tsunami generation.

Thermal Data

The most important constraints for our thermal models are the observed surface heat flows. *Lewis et al.* [1988], *Hyndman and Wang* [1993] and *Wang et al.* [1995] have summarized the extensive marine and land data for the southern Vancouver Island margin (Figure 12). There also is an Ocean Drilling Program (ODP) borehole value on the midcontinental slope [*Westbrook et al.*, 1994]. The thermally controlled subbottom depth to a gas-hydrate reflector (bottom-simulating reflector or BSR) provides important constraint for the critical continental slope region [*Hyndman et al.*, 1993]. Fewer marine probe and BSR data are available to the south; marine probe data have been presented by *Langseth and Hobart* [1984] (also *Shi et al.* [1988]) off Washington and *Korgen et al.* [1971] off Oregon. Also off Oregon, *Trehu et al.* [1995b] gave heat flow estimates from the depth of the BSR, and *Westbrook et al.* [1994] gave heat flow from an ODP drill hole near the top of the continental slope. The latter estimate has been revised to 70 mW m^{-2} based on long-term downhole temperature recording [*Davis et al.*, 1995]. All of the marine data have large uncertainties; the continental slope sediments are difficult to penetrate with the marine probe, and the early measurements of *Korgen et al.* [1971] employed only three temperature sensors. The ODP hole off Oregon penetrated a fault zone with inferred upward fluid flow. The BSR data have relatively large error estimates because of the uncertainty as to which hydrate stability field is applicable and in the physical properties of the sediments above the BSR. The continental slope heat flow may also be significantly disturbed by tectonically driven sediment thickening and fluid flow processes within the sedimentary accretionary prism [e.g., *Shi et al.*, 1988; *Hyndman et al.*, 1993]. The marine data have a large scatter, but otherwise there is a general decrease in heat flow landward from the high values in Cascadia Basin expected for 6-8 Ma crust (Figures 12 and 13).

The land data for western Washington and Oregon have been taken from the Decade of North American Geology (DNAG) compilation of North American heat flow [*Blackwell et al.*, 1989]. Most of the data come from the articles by *Blackwell et al.* [1990a, b] and *Blackwell et al.* [1981]. The land heat flow increases abruptly 10-20 km seaward of the line joining the major volcanic centers. Only data seaward of this boundary are presented here (about 280 km from the deformation front in northern Washington, about 240 km in southern Oregon). The land data within 100 km of the coast are consistently low as expected for a forearc setting; most are in the range 35-45 mW m^{-2} (mean 38.3 mW m^{-2}, s.d. 5.0 mW m^{-2}) (Figure 13). The underthrusting oceanic crust provides a substantial heat sink. The data do not allow clear discrimination of the heat flow variations along the margins of Washington and Oregon associated with variation in plate dip as predicted by our models. Therefore we have included all of the land and marine data projected onto a single profile for comparison with the model results.

Estimates of the radioactive heat generation and of thermal conductivity as functions of depth are critical model parameters. The thermal conductivity of the sediments in the accretionary prism has been taken to increase with depth from a value of 1.0 W m^{-1} K^{-1} near the seafloor to 2.0 W m^{-1} K^{-1} at a depth of 10 km. The sediment heat generation has been estimated from measurements on samples from Vancouver Island shelf wells to be 0.6 μW m^{-3}, which is similar to the average for the continental forearc rocks from which they have been eroded [*Lewis and Bentkowski*, 1988]. Thermal conductivity measurements on the Crescent/Siletz basaltic terrane have been obtained from a number of land sites in Washington and Oregon [*Blackwell et al.*, 1990a, b]; it is taken to be 1.59 W m^{-1} K^{-1} increasing to 2.0 downward. The radioactive heat generation is very small for these rocks, <0.1 μW m^{-3}, and it has been neglected. Our model temperatures in the region of interest are not very sensitive to the thermal conductivity of the continental rocks farther landward, and we have used a value of 3.0 W m^{-1} K^{-1} decreasing downward to 2.0 as a consequence of increasing temperature. Most of the rocks that have been measured in the forearc region are of low heat generation [e.g., *Lewis and Bentkowski*, 1988]; we have taken three layers decreasing downward of 0.6, 0.4, and 0.1 μW m^{-3}. This variation with depth approximates the commonly inferred exponential downward decrease in heat generation.

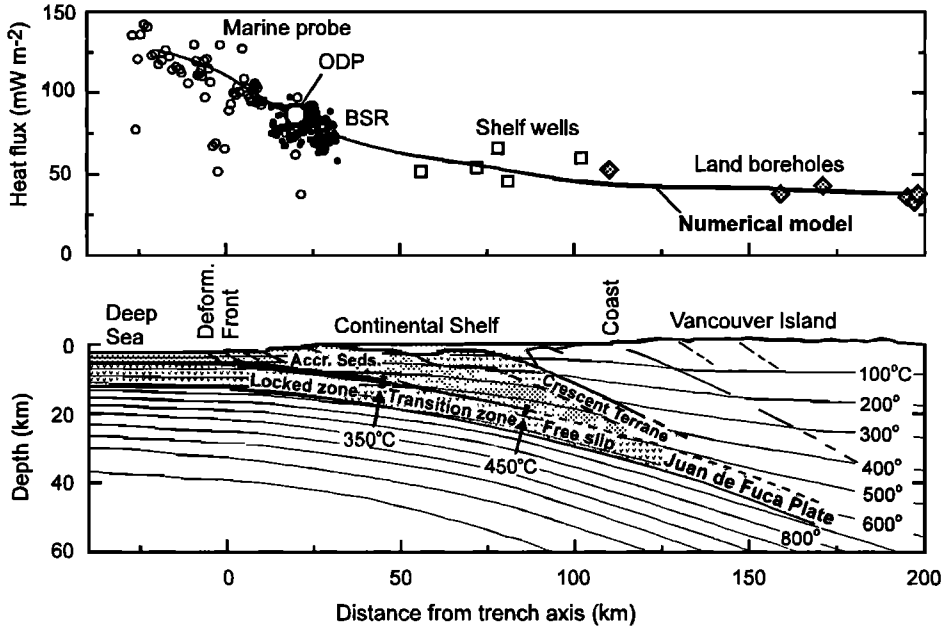

Figure 12. (top) Heat flow data along the southern Vancouver Island model profile and the predicted heat flow from the preferred numerical thermal model. (bottom) Thermal field from the numerical model along the profile superimposed on a structural cross section. The locked, transition, and free slip zones are illustrated.

Numerical Thermal Models

We have chosen to model the thermal regime numerically. Analytic expressions [e.g., *Molnar and England*, 1990; *Tichelaar and Ruff*, 1993] facilitate determining the sensitivity of the thermal field to various model parameters. However, they do not allow the complex structure and thermal properties variations that our detailed site-specific analyses require. We have previously described our numerical technique [*Hyndman and Wang*, 1993; *Hyndman et al.*, 1995; *Wang et al.*, 1995], and here we provide only a summary. We have solved the thermal equation for a steady state underthrusting slab using the finite element method [*Hyndman and Wang*, 1993]. Within each element, the thermal property values are uniform but the temperature may vary quadratically. A layer of very thin elements is used immediately below the surface to allow accurate calculation of surface heat fluxes.

The temperatures and thus the downdip extent of the locked seismogenic zone on the subduction thrust fault are very dependent on the local subduction parameters: (1) the age of the subducting plate, (2) the plate convergence rate, (3) the thickness of insulating sediments on the incoming crust, and (4) the dip angle profile of the fault. The thermal conductivity and upper layer heat generation of the overlying material strongly affect the surface heat flow, but they have a relatively small effect on the thrust fault temperature. The main parameters are given in the text above. In our model the detachment is taken at the top of the oceanic crust so that the subduction thrust temperatures at the deformation front are those calculated for the base of the incoming sediment section. This is a reasonable approximation at the locations of many of the Cascadia margin multichannel seismic profiles but as noted above, a few show detachments up to 1 km higher. This difference is important for temperatures on the thrust plane beneath the lower continental slope but should not be important for our main region of interest at the downdip end of the locked zone. The age of the underthrusting plate and the convergence rate have changed little over the past several tens of millions of years [*Riddihough*, 1982; *Engebretson et al.*, 1985] so a steady state solution is adequate. The temperature-depth profile for the sediment and the oceanic lithosphere at the deformation front has also been computed numerically employing the theory for a simple cooling plate and for the thermal effects of sedimentation [*Hyndman and Wang*, 1993]. We have ignored the thermal effect of the progressive thickening of the accretionary sedimentary prism. The sediment accretion and associated fluid expulsion reduce the temperatures beneath the continental slope but have little effect farther landward [*Wang et al.*, 1993; *Hyndman et al.*, 1993]. We have also ignored the thermal effect of uplift and erosion of the Olympic mountains on the northern Washington profile. Our previous model results showed that the predicted heat flow much exceeds that observed if there is significant frictional heating on

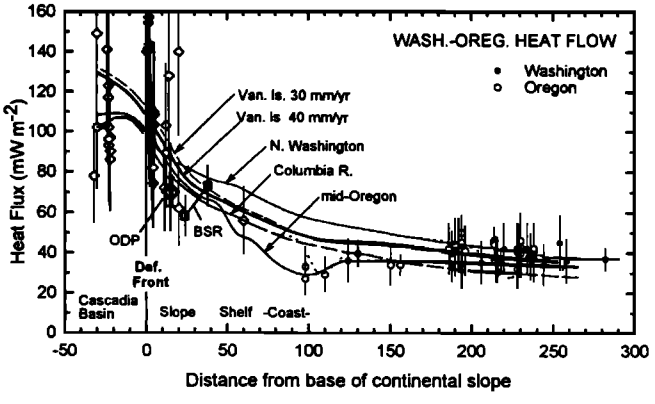

Figure 13. Heat flow data for Washington (solid symbols) and Oregon (open symbols) compared to the predicted heat flow from the numerical thermal models for each profile.

the subduction thrust fault [*Hyndman and Wang*, 1993; *Wang et al.*, 1995]. In Figures 12 and 13 we show only the results for models in which frictional heating has been neglected.

Model Results

We provide thermal model cross sections across the margin for three new profiles, northern Washington (Olympic Peninsula), Columbia River (Oregon-Washington border), and central Oregon. We have previously modeled the southern Vancouver Island margin [*Hyndman and Wang*, 1993; *Wang et al.*, 1994]; a summary is given in Figure 12. The thermally estimated locked and transition zones are 40 km and 60 km, respectively, slightly narrower than those estimated from the current deformation data. We have not modeled the northern California region. It is tectonically complex and requires a detailed separate analysis. In Figure 14 we show plots of model downdip temperatures on the subduction thrust as a function of landward distance for all four of our model profiles. The differences in predicted surface heat flows along the margin are primarily a consequence of variations of two factors, the thrust dip angle and the thermal conductivity of the overlying crust. The effect of shallow dip is illustrated by the northern Washington model. The predicted heat flow is much higher than for the other profiles. The downdip temperatures are much lower on this model profile so the predicted seismogenic zone is wider. The effect of low thermal conductivity in the overlying continental crust is illustrated by the mid-Oregon model profile. The low thermal conductivity Siletz/Crescent basalts extend to near the edge of the continental shelf on this profile [e.g., *Trehu et al.*, 1995a; *Hittleman et al.*, 1989], and their presence decreases the model heat flow substantially on the shelf and coastal region. In contrast to the effect of shallow thrust dip, the low thermal conductivity has only a small effect on the thrust temperatures. The low conductivity decreases the heat flow such that the vertical temperature gradient is little changed. The basalts extend along the whole Cascadia margin, but they have little effect on the other profiles since they do not extend as far seaward and they are inferred to be thinner. The effect of thermal refraction at the seaward and landward edges of the low conductivity basalts is evident in the detailed model heat flow profiles, but the transition is probably more gradual than modeled to give smoother real landward heat flow variation.

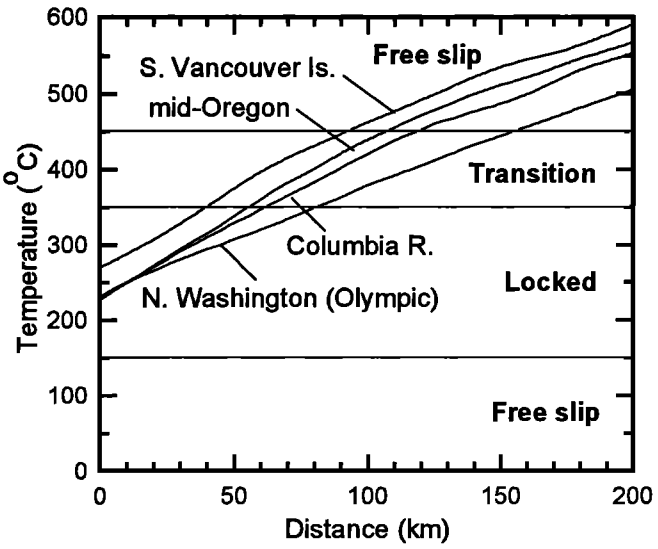

Figure 14. Model temperatures on the subduction thrust plane with landward distance from the base of the continental slope for southern Vancouver Island, northern Washington, Columbia River, and mid-Oregon. The downdip limits of the locked and transition zones are taken to be 350°C and 450°C. There may be free slip at temperatures below 150°C.

Northern Washington (Olympic) profile. The accretionary prism extends over the subduction thrust fault for most of the length of the northern Washington (Olympic) thermal profile. Thus the heat generation and thermal conductivity of the continental crust have no effect on the thrust fault temperatures in the region of interest. These parameters only affect the model heat flow east of about 250 km from the deformation front. Figure 13 shows the unusually slow decrease in predicted heat flow with distance landward resulting from the shallow thrust dip. The subducting slab has a smaller downward component of motion and thus provides a smaller heat sink compared to the steeper slabs to the north and south. The near-coast heat flow data that are closest to this profile are about 60 km to the south, close to the seaward end of the Westport-Aberdeen-Olympia leveling line (Figure 3), where the dip is steeper and thus the predicted heat flow is lower. The three values in this latter area (solid dots Figure 13), however, are higher than the six values near the Oregon coast (open circles, Figure 13) where the predicted heat flow is much lower. The predicted widths of the locked and transition zones (to 350° and 450°C) for this profile from the thermal model are 85 + 75 km (Figure 14), which is slightly narrower than the estimates from current deformation.

Columbia River profile. The Columbia River thermal profile also has accreted sediments for about 100 km landward of the deformation front so the model thrust temperatures in the area of interest are not affected by the continental crust. The predicted heat flow is dependent on the crustal heat generation and conductivity only east of about 120 km. The predicted widths of the locked and transition zones for this profile are 60 + 50 km (Figure 14), very close to the values from the analysis of current deformation. There is a substantial uncertainty because of the poorly known dip profile of the thrust fault.

Mid-Oregon profile. The mid-Oregon thermal profile has thick low thermal conductivity and low heat generation basalts (Siletz/Crescent) extending to near the edge of the continental shelf, only 50 km from the deformation front. As noted above, the basalts increase, but not greatly, the predicted thrust fault temperatures. Their presence reduces the width of the model locked zone by 5-10 km. However, the basalts substantially reduce the predicted heat flow in the coastal region. Three heat flow measurements near the central Oregon coast [*Blackwell et al.*, 1990b] show low values consistent with the model prediction (Figure 13). Unfortunately, these measurements have large uncertainties; for two of the sites the boreholes were less than 100 m deep, and for all three sites the thermal conductivities could only be estimated using samples from nearby areas. The predicted widths of the locked and transition zones are 50 + 40 km (Figure 14), which are wider than the predictions from the current deformation analysis (35 km +35 km). There are large uncertainties in the widths because of the dip profile of the thrust is not well constrained. We note that a thrust profile only about 3° steeper is required to give a thermally predicted seismogenic zone of 35-40 km as estimated from the current deformation data.

Summary of Thermal Constraints

Our numerical model results give good matches to the observed landward decreases in heat flow. The decrease is more

gradual for the shallower dip of the northern Washington (Olympic) margin; on this profile the downward component of subducting plate motion is much less than for the other profiles. Thus, on this profile the critical temperatures are reached much farther landward. The values of continental heat generation and thermal conductivity have a strong effect on the predicted heat flow, but only landward of the area of interest for most of the profiles. The exception is mid-Oregon where the low thermal conductivity Siletz/Crescent basalts extend much farther seaward compared to the other profiles and generate higher model thrust temperatures. The effect of the low conductivity, however, is not as large as might be expected because of the nearly balancing heat flow reduction. The younger plate age for the southern Vancouver Island profile results in higher model thrust temperatures and thus a narrower seismogenic zone. The other important parameters of sediment thickness on the incoming plate and the convergence rate do not vary enough among the profiles to significantly vary either the model heat flow or thrust fault temperatures.

The uncertainties in the positions of the critical temperatures of 350°C and 450°C cannot be determined rigorously. However, sensitivity tests that vary the main model parameters over reasonable ranges give downdip positions of these temperatures that vary by about ±20 km. The uncertainties are larger for the Columbia River and mid-Oregon profiles because of the poorly known subduction thrust dip profiles. The uncertainties on the width of the seismogenic zones from the thermal analysis are thus larger than from the deformation analysis. However, the locked and transition zone widths from the thermal analysis correspond to those from the deformation data within the estimated uncertainties (Figure 15). The largest discrepancy is for the central Oregon profile where the thermally estimated widths are greater than those from the analysis of current deformation, although they still agree to within the uncertainties. The narrowest zones from the thermal analysis are for the southern Vancouver Island profile where the incoming plate is younger than for the profiles to the south.

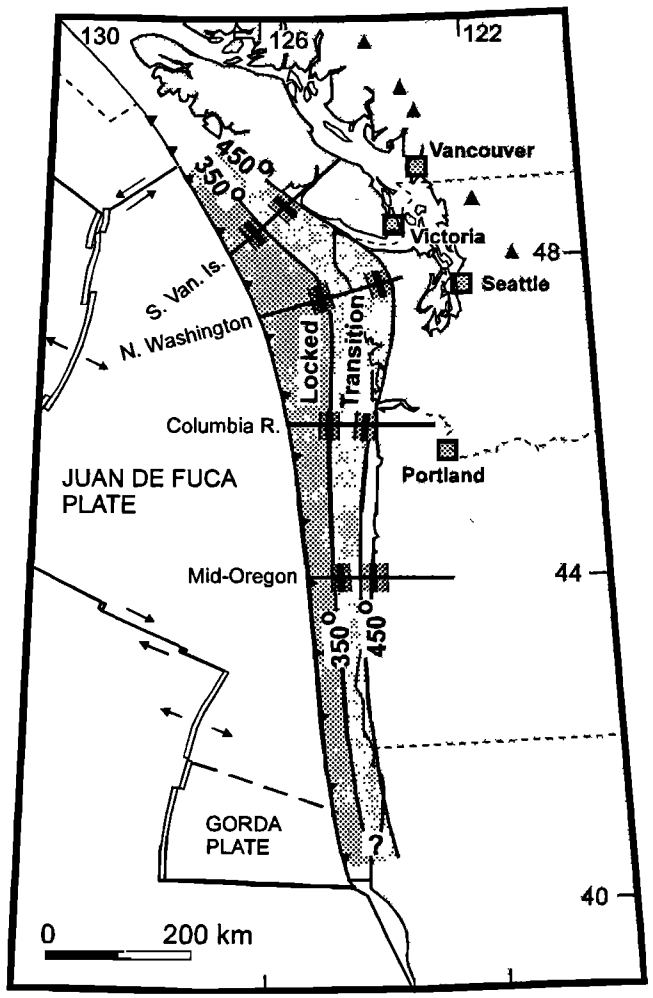

Figure 15. The widths of the locked and transition zones from the thermal analysis (thick short lines) compared to those from the current deformation (stippled areas). The bands on the thermal results (350 and 450°C) indicate the estimated uncertainties.

Discussion

Along the Cascadia margin, releveling, tide gauge, and gravity data indicate present uplift of the coast at rates of a few millimeters per year, decreasing inland. From positional surveys there is shortening across the coastal region at about 0.1 μstrain/yr (10 mm/yr per 100 km). The present interseismic uplift is in general agreement with the great earthquake coseismic subsidence inferred from buried coastal intertidal marshes and other paleoseismicity data. The current deformation data constrain the dislocation model widths for most of the Cascadia subduction zone margin with a resolution of about ±15%, or about ±10 km for 60 + 60 km locked and transition zone widths. The model locked and transition zones range from 35 + 35 km for the central Oregon to northern California margin, to 90 + 90 km for the northern Washington profile. The southern Vancouver Island margin has widths of 60 + 60 km. The inferred deformation pattern is remarkably simple. Although there are many local small-scale variations in the leveling and other current deformation data, none appear to be significant within the estimated uncertainties. Our interpretation of the current deformation data shows all of the Cascadia subduction fault to be locked.

The thermal model results indicate that the Cascadia locked zone is narrow because of unusually high temperatures. The maximum temperature for seismogenic behavior is reached an unusually short distance downdip on the subduction thrust fault compared to most subduction zones. The thermal constraints to the locked seismogenic zone have lower resolution than those from current deformation. The uncertainty in the downdip position of the critical temperatures (i.e., 350°C and 450°C) is about ±30%, i.e., ±20 km for 60 + 60 km locked and transition zone widths for the portions of the margin where the dip profile is well constrained. The uncertainty is larger for central Oregon because of the greater uncertainties in the dip profile. The uncertainties in the values of the critical temperatures are poorly known both in terms of average values and of variability due to rock compositions and state and due to strain rate. The uncertainties are undoubtedly at least a few tens of degrees Celsius or 10-20 km. The variations in estimated width of the locked zone from deformation data follow the major variation in the thermal regime on the top of the downgoing plate, i.e., the shallow dip northern Washington profile has the widest seismogenic zone both from the thermal constraint and from the geodetic data. In all cases the correspondence between the deformation and thermal widths is within the uncertainty estimates. The anomalous feature of the low thermal conductivity Siletz/Crescent basalts extending across most of the shelf off central Oregon also introduces model temperature uncertainties.

The main factor controlling variations along the margin of the thrust plane downdip temperature and thus the width of the locked seismogenic zone is the dip profile. The younger subducting plate age off southern Vancouver Island and the low thermal conductivity overlying crust off central Oregon also have some effect. The variations among the profiles in the other controlling parameters for the thermal regime do not affect the predicted widths of the seismogenic zone significantly, i.e., convergence rate and the small differences in thickness of sediments on the incoming oceanic crust. To a first order, the temperature variation downdip on the thrust fault depends simply upon depth, but the thermal regime (as seen in the modeled landward heat flow profiles) is affected by the plate dip. The heat flow decreases landward more slowly for a shallow plate dip since the downgoing plate then provides less of a heat sink. The wider locked zone for the northern Washington profile associated with the shallow dip, and thus with slowly increasing fault depth inland, is partly balanced by the higher vertical temperature gradient. The assumed thermal conductivity of the overlying plate affects the model heat flow substantially but, as shown for Oregon has a surprisingly small effect on the model thrust temperatures.

An important general conclusion from our thermal analysis is that each subduction zone margin must be modeled in detail to accurately estimate the width of the locked seismogenic zone. Generic analytic thermal solutions provide only limited constraint. The general correlations from the thermal analysis are that margins with steep thrust dip, young subducting lithosphere, slow convergence, and thick sediments on the incoming oceanic crust should have the narrowest locked seismogenic zones. As a comparison, we show a summary of the leveling data for a profile across southwest Japan with the corresponding dislocation model [*Hyndman et al.*, 1995] and a summary of the leveling data for northern Cascadia with the corresponding dislocation model (Figure 16). In each case the model locked and transition zone widths agree well with the predictions from thermal modeling taking the critical temperatures to be 350°C and 450°C.

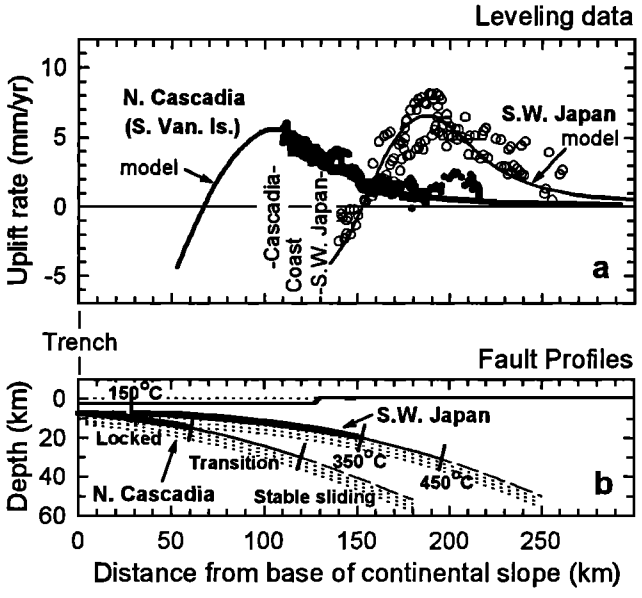

Figure 16. (a) Repeated leveling data for the mid interseismic period across the margin of SW Japan and across the northern Cascadia margin, compared to the vertical motion profiles from the preferred elastic dislocation models. (b) Cross sections of the SW Japan and northern Cascadia subduction thrust faults showing the locked, transition and stable sliding zones, along with the points where temperatures of 350°C and 450°C are reached.

Previous studies, especially for the Nankai margin of southwest Japan, have shown that the locked portion of the subduction thrust may be estimated by elastic dislocation modeling of the interseismic deformation and that the maximum downdip extent of seismic rupture corresponds well to the limit of the locked zone as estimated both before and after the most recent events. Fault slip appears to extend a few tens of kilometers downdip over a period of a few years following a great earthquake. As discussed above, further study is needed to give a solid theoretical foundation to the empirical agreement between the locked zone from simple dislocation modeling of the interseismic deformation and the coseismic rupture zone.

The seaward limit to the locked seismogenic zone is poorly constrained. If our hypothesis is correct that the controlling factor is the dehydration of stable sliding clays at about 150°C, the seaward limit for Cascadia is at the deformation front. This hypothesis has some support from studies of the southwest Japan margin, but it has not been convincingly tested. The seaward limit to the locked seismogenic zone is only important for earthquake hazard on land if the updip aseismic zone is sufficiently wide such as to significantly reduce the rupture zone width. The seaward limit, however, is important for the tsunami hazard.

The landward limit to the seismogenic zone, extending little if at all beneath the coast, limits the ground motion from great subduction earthquakes at the larger Cascadia cities that lie 100-200 km inland. The narrow width also limits the maximum earthquake size (the actual maximum depends on the along-margin length), but events of magnitude well over 8 are still expected. The very long thin aspect ratio represented by simultaneous rupture of the whole Cascadia locked zone would be exceptional based on past great earthquakes globally. However, taking the extreme case of a fault area of 90,000 km^2 (i.e., a fault length of 1000 km, the whole length of the Cascadia margin, by 90 km, the average width of the locked plus half the transition zone) the empirical moment magnitude versus rupture area relation of *Wells and Coppersmith* [1994] gives a maximum magnitude of M=8.9. The relation of *Wyss* [1979] gives a magnitude of M=9.1. Calculating the magnitude from the seismic moment (fault rupture displacement equal to the plate convergence rate over an average 590 year interval, i.e., 24 m) gives a maximum magnitude of 9.2.

Acknowledgments. J. Adams provided detailed data on earlier repeated leveling. C. Mitchell provided a manuscript copy with the more recent leveling and tide gauge data for southern Washington and for Oregon in advance of publication. D. Oleskevich undertook some of the thermal modeling. We acknowledge many helpful discussions with J. Adams, H. Dragert, G.C. Rogers, and E.E. Davis. B. Atwater provided a very helpful informal review of a preliminary manuscript. Geological Survey of Canada publication 47794.

References

Adams, J., Paleoseismicity of the Cascadia subduction zone: Evidence from turbidites off the Oregon-Washington margin, *Tectonics, 9*, 569-583, 1990.

Ando, M., and E.I. Balazs, Geodetic evidence for aseismic subduction of the Juan de Fuca plate, *J. Geophys. Res., 84*, 3023-3028, 1979.

Arnadottir, T., P. Segall, and M. Matthews, Resolving the discrepancy between geodetic and seismic fault models for the 1989 Loma Prieto, California earthquake, *Bull. Seism. Soc. Am., 82,* 2248-2255, 1992.

Atwater, B.F., Evidence for great Holocene earthquakes along the outer coast of Washington State, *Science, 236,* 942-944, 1990.

Atwater, B.F., et al., Consensus about past great earthquakes at the Cascadia subduction zone, *Earthquake Spectra,* 11, 1-18, 1995.

Barrientos, S.E., and G. Plafker, Postseismic coastal uplift in southern Chile, *Geophys. Res. Lett., 19,* 701-704, 1992.

Blackwell, D.D., R.G. Bowen, D.A. Hull, J. Riccio, and J.L. Steele, Heat flow, arc volcanism and subduction in northern Oregon, *J. Geophys. Res., 87,* 8735-8754, 1981.

Blackwell, D.D., J.L. Steele, and L.C. Carter, Heat flow data base for the United States, in *Geophysics of North America CD-ROM,* edited by A.M. Hittleman, J.O. Kinsfather, and H. Meyers, NOAA, Nat. Geophys. Data Cent., Boulder, Colo., 1989.

Blackwell, D.D., J.L. Steele, M.K. Frohme, C.F. Murphey, G.R. Priest, and G.L. Black, Heat flow in the Oregon Cascade range and its correlation with regional gravity, Curie point depths, and Geology, *J. Geophys. Res., 95,* 19,475-19,493, 1990a.

Blackwell, D.D., J.L. Steele, and S. Kelley, Heat flow in the state of Washington and thermal conditions in the Cascade Range, *J. Geophys. Res., 95,* 19,495-19,516, 1990b.

Bostock, M.G., and J.C. VanDecar, Upper mantle structure of the northern Cascadia subduction zone, *Can. J. Earth Sci., 32,* 1-12, 1995.

Brown, L.D., and J.E. Oliver, Vertical crustal movements from leveling data and their relation to geologic structures in the eastern United States, *Rev. Geophys., 14,* 13-35, 1976.

Byrne, D.E., D.M. Davis, and L.R. Sykes, Loci and maximum size of thrust earthquakes and the mechanics of the shallow region of subduction zones, *Tectonics, 7,* 833-857, 1988.

Cassidy, J., A review of receiver function studies in the southern Canadian Cordillera, *Can. J. Earth. Sci.*, in press, 1995.

Cassidy, J., and R.M. Ellis, S wave velocity structure of the northern Cascadia subduction zone, *J. Geophys. Res., 98,* 4407-4421, 1993.

Clague, J.J., and P.T. Bobrowsky, Evidence for a large earthquake and tsunami 200-400 years ago on western Vancouver Island, British Columbia, *Quat. Res., 41,* 176-184, 1994a.

Clague, J.J., and P.T. Bobrowsky, Tsunami deposits in tidal marshes on Vancouver Island, British Columbia, *Geol. Soc. Am. Bull., 106,* 1293-1303, 1994b.

Clague, J.J., J.R. Harper, R.J. Hebda, and D.E. Howes, Late Quaternary sea levels and crustal movements, coastal British Columbia, *Can. J. Earth. Sci., 19,* 597-618, 1982.

Crosson, R.S., and T.J. Owens, Slab geometry of the Cascadia subduction zone beneath Washington from earthquake hypocenters and teleseismic converted waves, *Geophys. Res. Lett., 14,* 824-827, 1987.

Davis, E.E., and R.D. Hyndman, Accretion and recent deformation of sediments along the northern Cascadia subduction zone, *Geol. Soc. Am. Bull., 101,* 1465-1480, 1989.

Davis, E.E., K. Becker, K. Wang, and B. Carson, Long-term observations of pressure and temperature in hole 892B, Cascadia accretionary prism, *Proc. Ocean Drill. Program, Sci. Results, 146 (Part 2),* in press, 1995.

DeMets, C., R.G. Gordon, D.F. Argus, and S. Stein, Current plate motions, *Geophys. J. Int.*, 101, 425-478, 1990.

Douglas, B.C., Global sea level rise, *J. Geophys. Res., 96,* 6981-6992, 1991.

Dragert, H., and R.D. Hyndman, Continuous GPS monitoring of strain in the northern Cascadia subduction zone, *Geophys. Res. Lett., 22,* 755-758, 1995.

Dragert, H., and M. Lisowski, Crustal deformation measurements on Vancouver Island, British Columbia: 1976 to 1988, in *Global and Regional Geodynamics,* edited by P.Vyskocil, C. Reigber, and P.A. Cross, pp. 241-250, Springer-Verlag, New York, 1990.

Dragert, H., R.D. Hyndman, G.C. Rogers, and K. Wang, Current deformation and the width of the seismogenic zone of the northern Cascadia subduction thrust, *J. Geophys. Res., 99,* 653-668, 1994.

Engebretson, D.C., A. Cox, and G.A. Thompson, Relative motions between oceanic and continental plates in the Pacific Basin, *Spec. Pap. Geol. Soc. Am., 196,* 59 pp., 1985.

Guibault, J-P., J.J. Clague, and M. Lapointe, The use of foraminifera in estimating coseismic subsidence: An example from Vancouver Island, British Columbia, *Geol. Soc. Am.*, 1994 Annual Meeting, Abstr. Programs, p. 144, 1994.

Hicks, S.D., An average geopotential for the United States, *J. Geophys. Res., 83,* 1377-1379, 1978.

Hittleman, A.M., J.O. Kinsfather, and H. Meyers (Eds.), *Geophysics of North America CD-ROM,* NOAA, Nat. Geophys. Data Cent., Boulder, Colo., 1989.

Holdahl, S.R., R. Faucher, and H. Dragert, Contemporary vertical crustal motion in the Pacific Northwest, in *Slow Deformation and Transmission of Stress in the Earth, Geophys. Monogr. Ser.*, vol. 49, edited by S.C. Cohen and P. Vanicek, pp. 17-29, AGU, Washington, D.C., 1989.

Hyndman, R.D., and K. Wang, Thermal Constraints on the zone of major thrust earthquake failure: The Cascadia subduction zone, *J. Geophys. Res., 98,* 2039-2060, 1993.

Hyndman, R.D., C.J. Yorath, R.M. Clowes, and E.E. Davis, The northern Cascadia subduction zone at Vancouver Island: Seismic structure and tectonic history, *Can. J. Earth Sci., 27,* 313-329, 1990.

Hyndman, R.D., K. Wang, T. Yuan, and G.D. Spence, Tectonic sediment thickening, fluid expulsion, and the thermal regime of subduction zone accretionary prisms: The Cascadia margin off Vancouver Island, *J. Geophys. Res., 98,* 21,865-21,876, 1993.

Hyndman, R.D., G.D. Spence, T. Yuan, and E.E. Davis, Regional geophysics and structural framework of the Vancouver Island margin accretionary prism, Proc. Ocean Drill. Program, Initial Rep., *146,* 399-419, 1994.

Hyndman, R.D., K. Wang, and M. Yamano, Thermal constraints to the seismogenic portion of the southwestern Japan subduction thrust, *J. Geophys. Res.*, in press, 1995.

Kelsey, H.M., D.C. Engebretson, C.E. Mitchell, and R.L. Ticknor, Topographic form of the Coast Ranges of the Cascadia margin in relation to coastal uplift rates and plate subduction, *J. Geophys. Res., 99,* 12,245-12,255, 1994.

Korgen, B.J., G. Bodvarsson, and R.S. Mesecar, Heat flow through the floor of the Cascadia Basin, *J. Geophys. Res., 76,* 4758-4774, 1971.

Langseth, M.G. and M.A. Hobart, A marine geothermal study over deformed sediments of the subduction complex off Oregon and Washington (abstract), *Eos Trans. AGU, 65,* 1089, 1984.

Lewis, T.J., and W.H. Bentkowski, Potassium, uranium and thorium concentrations of crustal rocks: A data file, *Geol. Surv. Can. Open File Rep., 1744,* 1988.

Lewis, T.J. W.H. Bentkowski, E.E. Davis, R.D. Hyndman, J.G. Souther, and J.A. Wright, Subduction of the Juan de Fuca plate: Thermal consequences, *J. Geophys. Res., 93,* 15,207-15,225, 1988.

Lisowski, M., W.H. Prescott, H. Dragert, and S.R. Holdahl, Results from 1986 and 1987 GPS survey across the Strait of Juan de Fuca, Washington and British Columbia (abstract), *Seismol. Res. Lett., 60,* 1, 1989.

MacKay, M.E., G.F. Moore, G.R. Cochrane, J.C. Moore, and L.D. Kulm, Landward vergence and oblique structural trends in the Oregon margin accretionary prism: implications and effect on fluid flow, *Earth Planet. Sci. Lett., 109,* 477-491, 1992.

Mitchell, C.E., Vertical component of present-day deformation in the western Pacific Northwest, M.Sc. thesis, 103 pp., Univ. of Oreg., Eugene, 1992.

Mitchell, C.E., P. Vincent, R.J. Weldon II, and M.A. Richards, Present-day vertical deformation of the Cascadia margin, Pacific Northwest, U.S.A., *J. Geophys. Res., 99,* 12,257-12,277, 1994.

Molnar, P., and P. England, Temperatures, heat flux, and frictional stress near major thrust faults, *J. Geophys. Res., 95*, 4833-4856, 1990.

Owens, T.J., R.S. Crosson, and M. A. Hendrickson, Constraints of the subduction geometry beneath western Washington from broadband teleseismic waveform modeling, *Bull. Seismol. Soc. Am., 78*, 1319-1334, 1988.

Peltier, W.R., Deglaciation-induced vertical motion of the North American continent, *J. Geophys. Res., 91*, 9099-9123, 1986.

Rasmussen, J., and E. Humphreys, Tomographic image of the Juan de Fuca plate beneath Washington and western Oregon using teleseismic *P*-wave travel times, *Geophys. Res. Lett., 15*, 1417-1420, 1988.

Reilinger, R., and J. Adams, Geodetic evidence for active landward tilting of the Oregon and Washington coastal ranges, *Geophys. Res. Lett., 9*, 401-403, 1982.

Riddihough, R.P., Gorda plate motions from magnetic anomaly analysis, *Earth Planet. Sci. Lett., 51*, 163-170, 1980.

Riddihough, R.P., Contemporary movements and tectonics on Canada's west coast: A discussion, *Tectonophysics, 86*, 319-341, 1982.

Riddihough, R.P., Recent movements of the Juan de Fuca plate system, *J. Geophys. Res., 89*, 6980-6994, 1984.

Rieken, E., and R.L. Thiessen, Three-dimensional model of the Cascadia subduction zone using earthquake hypocenters, western Washington, *Bull. Seism. Soc. Am., 82*, 2533-2548, 1992.

Savage, J.C., A dislocation model of strain accumulation and release at a subduction zone, *J. Geophys. Res., 88*, 4984-4996, 1983.

Savage, J.C., and G. Plafker, Tide gage measurements of uplift along the south coast of Alaska, *J. Geophys. Res., 96*, 4325-4335, 1991.

Savage, J.C., M. Lisowski, and W.H. Prescott, Geodetic strain measurements in Washington, *J. Geophys. Res., 86*, 4929-4940, 1981.

Savage, J.C., M. Lisowski, and W.H. Prescott, Strain accumulation in western Washington, *J. Geophys. Res., 96*, 14,493-14,507, 1991.

Scholtz, C.H., *Mechanics of Earthquakes and Faulting*, 439 pp., Cambridge Univ. Press, New York, 1990.

Shi, Y., C-Y. Wang, M.G. Langseth, M. Hobart, and R. von Huene, Heat flow and thermal structure of the Washington-Oregon Accretionary prism -- A study of the lower slope, *Geophys. Res. Lett., 15*, 1113-1116, 1988.

Smith, S.W., and J.S. Knapp, Seismicity of the Gorda plate, structure of the continental margin, and an eastward jump of the Mendocino triple junction, *J. Geophys. Res., 98*, 8153-8171, 1993.

Snavely, P.D., Tertiary geologic framework, neotectonics, and petroleum potential of the Oregon-Washington continental margin, in *Geology and Resource Potential of the Continental Margin of Western North America and Adjacent Ocean Basins - Beaufort Sea to Baja California, Earth Sci. Ser.*, vol. 6, pp. 305-336, Circum-Pac. Counc. for Energy and Miner. Resour., Houston, Tex., 1987.

Snavely, P.D., and H.C. Wagner, Geologic cross section across the continental margin off Cape Flattery, Washington, *U.S. Geol. Surv. Open File Rep. 81-0978*, 1981.

Snay, R.A., and T. Matsikari, Horizontal deformation in the Cascadia subduction zone as derived from serendipitous geodetic data, *Tectonophysics, 194*, 59-67, 1991.

Spence, G.D., R.D. Hyndman, E.E. Davis, and C.J. Yorath, Seismic structure of the northern Cascadia accretionary prism: Evidence from new multichannel seismic reflection data, in *Continental Lithosphere: Deep Seismic Reflections, Geodyn. Ser.*, vol. 22, edited by R. Meissner et al., pp. 257-263, AGU, Washington, D.C., 1991.

Thatcher, W., The earthquake deformation cycle at the Nankai Trough, southwest Japan, *J. Geophys. Res., 89*, 3087-3101, 1984.

Thatcher, W., and J.B. Rundle, A viscoelastic coupling model for the cyclic deformation due to periodically repeated earthquakes at subduction zones, *J. Geophys. Res., 89*, 7631-7640, 1984.

Tichelaar, B.W., and L.J. Ruff, Depth of seismic coupling along subduction zones, *J. Geophys. Res., 98*, 2017-2037, 1993.

Trehu, A., I. Asudeh, T. Brocher, J. Luetgert, W. Mooney, J. Nabelek, and Y. Nakamura, Crustal architecture of the Cascadia forearc beneath northwestern Oregon, *Science*, in press, 1995a.

Trehu, A., G. Lin, E. Maxwell, and C. Goldfinger, A seismic reflection profile across the Cascadia subduction zone offshore central Oregon: New constraints on methane distribution and crustal structure, *J. Geophys. Res.*, in press, 1995b.

Trupin, A., and J. Wahr, spectroscopic analysis of global tide gauge sea level data, *Geophys. J. Int., 100*, 441-453, 1990.

Vanicek, P., R.O. Castle, and E.I. Balazs, Geodetic levelling and its applications, *Rev. Geophys., 18*, 505-524, 1980.

Vincent, P., Geodetic deformation of the Oregon Cascadia margin, M.Sc. thesis, 86 pp., Univ. of Oreg., Eugene, 1989.

Vrolijk, P., On the mechanical role of smectite in subduction zones, *Geology, 18*, 703-707, 1990.

Wang, C.Y., Sediment subduction and frictional sliding in a subduction zone, *Geology, 8*, 530-533, 1980.

Wang, K., and G.C. Rogers, Double seismic layers in the subducted Gorda plate and rheology of oceanic lithosphere, *Geophys. Res. Lett., 21*, 121-124, 1994.

Wang, K., R.D. Hyndman, and E.E. Davis, Thermal effects of sediment thickening and fluid expulsion in accretionary prisms, *J. Geophys. Res., 98*, 9975-9984, 1993.

Wang, K., H. Dragert, and H. J. Melosh, Finite element study of surface deformation in the northern Cascadia subduction zone, *Can. J. Earth Sci., 31*, 1510-1522, 1994.

Wang, K., T. Mulder, G.C. Rogers, and R.D. Hyndman, Case for very low coupling stress on the Cascadia subduction fault, *J. Geophys. Res., 100*, 12,907-12918, 1995.

Wells, D.L. and K.J. Coppersmith, New empirical relations among magnitude, rupture length, rupture width, rupture area, and surface displacement, *Bull. Seismol. Soc. Am., 84*, 974-1002, 1994.

Westbrook, et al., *Proceedings of the Ocean Drilling Program, Initial Reports*, vol. 146 (Part 1), 611 pp., Ocean Drill. Program, College Station Tex.,1994.

Wilson, D.S., Deformation of the so-called Gorda plate, *J. Geophys. Res., 94*, 3065-3075, 1989.

Wyss, M., Estimating maximum expectable magnitude of earthquakes from fault dimensions, *Geology, 7*, 336-340, 1979.

R.D. Hyndman and K. Wang, Pacific Geoscience Centre, Geological Survey of Canada, P.O. Box 6000, Sidney British Columbia, Canada V8L 4B2. (email: hyndman@pgc.emr.ca)

(Received December 9, 1994; revised June 19, 1995; accepted June 20, 1995.)